Fatigue of two oxide/oxide ceramic matrix composites at 1200°C in air and in steam. Effect of diamond-drilled effusion holes.

THESIS

Anthony Robert Cabri, 2d Lt, USAF

AFIT-ENY-MS-21-M-291

DEPARTMENT OF THE AIR FORCE
AIR UNIVERSITY

AIR FORCE INSTITUTE OF TECHNOLOGY

Wright-Patterson Air Force Base, Ohio

AFIT-ENY-MS-21-M-291

FATIGUE OF TWO OXIDE/OXIDE CERAMIC MATRIX COMPOSITES AT 1200°C IN AIR AND IN STEAM. EFFECT OF DIAMOND-DRILLED EFFUSION HOLES.

THESIS

Presented to the Faculty

Department of Aeronautics and Astronautics

Graduate School of Engineering and Management

Air Force Institute of Technology

Air University

Air Education and Training Command

in Partial Fulfillment of the Requirements for the

Degree of Master of Aeronautical Engineering

Anthony Robert Cabri, BS

2d Lt, USAF

March 25, 2021

AFIT-ENY-MS-21-M-291

FATIGUE OF TWO OXIDE/OXIDE CERAMIC MATRIX COMPOSITES AT 1200°C IN AIR AND IN STEAM. EFFECT OF DIAMOND-DRILLED EFFUSION HOLES.

THESIS

Anthony Robert Cabri, BS
2d Lt, USAF

Committee Membership:

Dr. Marina B. Ruggles-Wrenn, PhD
Chair

Dr. Randall S. Hay, PhD
Member

Dr. Eric L. Jones, PhD
Member

AFIT-ENY-MS-21-M-291

Abstract

The tension-tension fatigue behavior of two oxide-oxide ceramic matrix composites (CMCs) was investigated at 1200°C in laboratory air and in steam. Both composites consist of a porous oxide matrix reinforced with laminated, woven mullite/alumina (Nextel^{TM}720) fibers, have no interface between the fiber and matrix, and rely on the porous matrix for flaw tolerance. The first composite had an alumina matrix, while the second composite had an alumina-mullite matrix. The objectives of the present study were twofold. First, the effects of incorporating mullite into the matrix material on the composite's fatigue performance were assessed. To achieve this objective, the tension-tension fatigue behavior of the CMC with the alumina-mullite matrix was studied. The results were compared and contrasted with those previously obtained for the CMC with the alumina matrix. Second, the effects of an array of effusion holes on the fatigue performance of the CMC with the alumina matrix were determined. Specimens containing an array of 17 effusion holes of 0.5-mm diameter were tested in tension-tension fatigue. The effusion holes were drilled through the specimen thickness normal to the specimen surface using diamond tooling. To evaluate the additional effects of steam environment, all fatigue tests were conducted at 1200°C in laboratory air and in steam. All fatigue tests were performed at a frequency of 1.0 Hz with the ratio of minimum to maximum stress R = 0.05. The fatigue stress levels ranged from 100 to 150 MPa for the CMC with the alumina matrix, and from 10 to 140 MPa for the CMC with the alumina-mullite matrix. The fatigue run-out was set to 100,000 cycles. All specimens that achieved fatigue run-out were subjected to tension tests to failure in order to measure the retained tensile properties. Incorporation of mullite into the composite matrix had little effect on the composite fatigue per-

formance. However, the presence of the effusion holes caused degradation in fatigue resistance of the CMC with the alumina matrix in steam. Fracture surfaces of the tested specimens were examined, damage and failure mechanisms are discussed.

I dedicate this work to my parents, Greg and Susan.

"Be who you are and be that well..."

St. Francis de Sales

Acknowledgements

Foremost, I would like to express my sincere gratitude to my research advisor, Dr. Marina Ruggles-Wrenn, for her continuous support these past two years. I would like to thank the laboratory technicians, Mr. Mike Ranft and Mr. Jamie Smith, who made my tenure in the MTS Laboratory as efficient and productive as possible. I would like to thank my academic advisor, Dr. Anthony Palazotto, for welcoming me to AFIT and providing academic advice whenever necessary. And I would like to finally thank my family, especially my parents, for supporting me at every step of this journey.

Anthony Robert Cabri

Table of Contents

Page

List of Figures

List of Tables

FATIGUE OF TWO OXIDE/OXIDE CERAMIC MATRIX COMPOSITES AT 1200°C IN AIR AND IN STEAM. EFFECT OF DIAMOND-DRILLED EFFUSION HOLES.

I. Introduction

The desire to operate aerospace vehicles with greater efficiency than conventionally practiced has created a need for materials able to withstand aggressive operating environments. Advanced aerospace applications that call for advanced structural materials with superior long-term mechanical properties include hypersonic flight vehicles, aircraft turbine engine components, and spacecraft re-entry thermal protection systems. The candidate materials for these applications must withstand high temperatures, high pressures, as well as varying environmental factors, such as the presence of air or steam. Because of their low density and excellent high-temperature mechanical properties, ceramic matrix composites (CMCs) are being evaluated for aircraft engine hot-section components. In this application, the components must operate in a highly oxidizing combustion environment. Hence the thermodynamic stability and resistance to oxidative degradation of the candidate composites is a vital issue. Oxide-Oxide CMCs containing an oxide-fiber and oxide-matrix, are viable solutions for this type of application [16].

Before CMC parts can be placed into service, their structural integrity and long-term environmental durability must be assured. Characterization of candidate CMC mechanical behavior at relevant service temperatures and environmental conditions, is required. Previous research efforts at the Air Force Institute of Technology (AFIT) studied the high-temperature mechanical behavior of oxide/oxide CMCs as well as

that of several advanced silicon-carbide/silicon-carbide (SiC/SiC) CMCs [16][19][20][21]. Composites were subjected to complex sustained and cyclic loading histories including tension-compression fatigue and creep in interlaminar shear. Test temperatures ranged from 800°C to 1300°C in air and in steam. Additionally, prior research efforts at AFIT investigated effects of holes and notches on high-temperature mechanical behavior of the CMCs.

It is recognized that the oxide/oxide CMCs are designed specifically to exhibit flaw tolerance combined with oxidation resistance. Numerous research efforts at AFIT focused on studying mechanical behavior of N720/A and N720/AM material systems at elevated temperature in air and in steam. Such research is particularly relevant because these materials are a potential choice for applications experiencing high temperature, high pressure, moisture-containing environments. Prior work at AFIT demonstrated that the presence of steam significantly reduced creep resistance of both N720/A and N720/AM composites at elevated temperature [1][16]. In contrast, both N720/A and N720/AM composites exhibited exceptional fatigue performance at elevated temperature in laboratory air. Furthermore, effects of steam on fatigue performance were negligible at frequencies of 1.0 Hz and above [16][19][27].

In recent years, aircraft turbine engine designers have attempted to increase thrust capabilities by improving the engine thermodynamic efficiency. Specifically, designers have attempted to increase operating temperatures at the combustor exit and high-pressure turbine stage inlet. This alteration is a concern for materials scientists because the temperatures experienced in these engine sections are already very high and a significant increase in temperature would supersede the upper operating temperature limit for most CMCs. In order for CMCs to remain a viable material for these applications, internal cooling processes such as "film-cooling" would have to be implemented. Film-cooling is a process where cool air flowing from the compressor

stage is channeled to the more interior regions of the engine, where it is then released through small holes on a blade or vane to cool the localized area [17]. Film-cooling can be accomplished by manufacturing parts containing arrays of small holes that would allow cool air to escape the part's internal cavities during operation, travel over its surface and create a "film" of cooling air. Previous AFIT research efforts investigated the effects of diamond-drilled and laser-drilled effusion holes on tensile properties and tensile creep performance of N720/A composite at 1200°C in air and in steam [6][13]. Results demonstrated that creep resistance of the composite was reduced due to the presence of the effusion holes. The loss of creep resistance was particularly pronounced in the case of the laser-drilled holes.

The objectives of this research effort are multifold. The first objective is to assess the effects of the matrix material on the mechanical performance and environmental durability of an oxide/oxide CMC reinforced with Nextel^{TM} 720 fibers. The composite, N720/AM, consists of an alumina-mullite matrix reinforced with alumina-mullite Nextel^{TM}720 fibers. The tension-tension fatigue performance of the N720/AM composite is studied in ambient air at its maximum use temperature of 1200°C. The results complement prior studies at AFIT focused on mechanical behavior and environmental durability of oxide/oxide CMCs.

The second objective is to evaluate the effects of effusion holes on the fatigue durability of the N720/A CMC consisting of the pure alumina matrix reinforced with alumina-mullite Nextel^{TM} 720 fibers. Test specimens contain an array of small effusion holes drilled using diamond tooling. Tension-tension fatigue tests are performed at 1200°C in laboratory air and steam environments. The present effort complements previous studies at AFIT which focused on the effects of diamond-drilled and laser-drilled small holes on creep behavior of the N720/A CMC at 1200°C in air and in steam [6][13].

Additionally, this effort aims to explore the viability of using brazing to join the N720/A oxide/oxide CMC. The tensile strength of N720/A CMC specimens with a brazed joint is characterized at temperatures ranging from 23° to 650°C in laboratory air.

II. Literature Review

Ceramic Matrix Composites (CMCs) are one of few materials that retain strength properties at high temperature. Oxide/Oxide CMCs are a specific type of composite which in addition to retaining strength properties, are inherently oxidation resistant and are designed for use in high-temperature environments exposed to ambient air and oxygenated gases. These qualities make them very attractive to the aerospace community. Modifications can be made to these materials to better adapt them for their respective service environments. For example, internal cooling processes may necessitate materials be drilled or compact service environments may require unique material geometries. This literature review explores several CMCs that are viable materials for these unique service environments.

To understand the qualities of the Nextel^{TM} 720/A and Nextel^{TM} 720/AM specimens used for this research effort, it is important to understand several qualities about the material. Understanding the design and function of ceramic matrix composites (CMCs), focusing on specifically oxide/oxide CMCs, and examining the properties of N720/A's and N720/AM's fiber and matrix constituents, are essential for material characterization. Furthermore, an understanding of effusion holes, brazing, and their effect on CMC mechanical performance provides insight for material testing. Section 2.1 generally defines composite materials and explains where CMCs fall within that realm. Section 2.2 looks into oxide/oxide ceramic matrix composites, materials that were designed to combat oxidation and employed in environments introduced to ambient air and other oxygenated gases. Section 2.3 explores Nextel^{TM} 720/A and Nextel^{TM} 720/AM, elaborating on how the Nextel^{TM} fibers were designed and their intended uses as well as the materials' respective matrices. Section 2.4 focuses on Cusil Active Brazing Alloy (Cusil-ABA®), the braze used in this research effort to join two N720A species together. Section 2.5 looks into previous AFIT research efforts

of CMC testing including N720/A and N720/AM and their respective performances. Section 2.6 identifies the objectives of this research effort.

2.1 Ceramic Matrix Composites

A composite material is two or more separate materials combined into a singular structural unit. More specifically, a composite is a material with two or more chemically distinct constituents which have a unique interface and when combined, produce a new material with enhanced properties. The two constituents of a composite are its fiber and matrix. Together, they can be engineered to give the composite certain mechanical properties such as desired strength, toughness, brittleness, and failure modes. The fiber typically carries the majority of the load as many materials are stronger and stiffer in fiber form. The matrix helps distribute compressive loads, provides protection for the fibers, and provides structure for the composite. Particulate composites, fiber-reinforced polymers, metal-matrix composites, and ceramic matrix composites are the major types of engineering composites [7].

Ceramic matrix composites (CMCs) are known for their ability to maintain strength properties at high temperatures. Advanced aerospace structures such as hypersonic vehicles, space re-entry thermal protection systems, aircraft engines, and various land based turbines are several areas that can benefit from CMC application [2]. In comparison to the metallic alloys and superalloys conventionally used for aircraft parts, CMCs are lower density materials which can be used in higher-temperature environments. If used within jet engines, their weight and strength properties would allow engines to operate more efficiently at higher operating temperatures and at a lesser weight, translating to cleaner and cheaper air transportation. Figure 1 highlights potential areas for CMCs within an aviation turbine engine [11].

For most materials, the fabrication process limits part geometries because of com-

Figure 1. Potential CMC applications within a Turbine Engine [11]

plexity, cost, and weight. An alternative method for manufacturers is to fabricate several smaller parts and join the materials together. This approach can be used for ceramic matrix composites and thus characterization of joined material behavior is essential knowledge for system designers.

In addition to retaining strength properties at high temperatures, high toughness and non-catastrophic failure modes make them a desirable material for aggressive aerospace environments. To obtain a non-catastrophic failure mode, a weak fiber/-matrix interface is used to deflect crack growth and allow for fiber pullout. This design dissipates load energy during application and prevents fiber failure at lower applied stresses [16]. Introduction to ambient air can lead to oxidation of the material. If oxidation is present, the material lifetime is decreased significantly. Ceramic Matrix Composites can be categorized into two groups, oxide/oxide CMCs and Non-oxide/oxide CMCs. Oxide/Oxide CMCs are considered in this study and are desirable materials because of their natural oxidation resistance.

2.2 Oxide/Oxide CMCs and Oxidation

Oxide/Oxide CMCs were created to combat material oxidation in high-temperature air environments. Because aerospace systems are operating in a variety of areas, it

is very important that the materials chosen retain strength properties when incorporated with ambient air and other hot gases, such as the combustion reaction products carbon dioxide, water vapor, and others. Oxidation occurs when a molecule loses one or more electrons within a chemical reaction. Materials on the aerospace system come into contact with ambient air or the combustion products mentioned previously, and undergo serious changes on a molecular level. Oxidation's overarching impact is a premature catastrophic degradation of material performance and an alteration of material properties [26].

Oxide/Oxide CMCs (Ox/Ox) are a specific type of ceramic matrix composite that were designed as a solution for oxidation. Prior to the creation of ox/ox CMCs, Non- ox/ox CMCs such as Silicon-Carbide/Silicon-Carbide (SiC/SiC) materials were being used in high-temperature air environments and were oxidizing aggressively. Composite materials able to maintain thermodynamic stability as well as resist oxidation were greatly needed if composites were going to replace conventional alloys in these environments. To combat oxidation, engineers believed they could mitigate the problem by applying fiber coatings to non-oxidized materials or by using oxidized fiber and matrix materials. Applying fiber coatings would prevent the occurrence of oxidation for the lifetime of the coatings however, if coatings were worn away or if composites experienced coating mishaps during the fabrication process, oxidation would still occur. Alternatively, if composite constituents used were already oxidized, this would remove the possibility of oxidation altogether. These oxidized fiber and matrix materials, when synthesized, became known as oxide/oxide CMCs.

The bonding relationship between fiber and matrix of an ox/ox CMC determines how the material performs during loading. Non- oxide/oxide CMCs, or dense matrix composites, utilize a weak fiber/matrix interphase. A weak interphase insures that when materials are placed under load and cracks begin to form, a singular crack will

not quickly propagate through both fiber and matrix components and ultimately fail the material [29]. Seen in Figure 2, for conventional (weak interface) concepts, the matrix crack begins to propogate through the matrix first and propogates around the fibers. The load is transferred to the fibers completely once the matrix has failed and performance is dictated by the fiber [29].

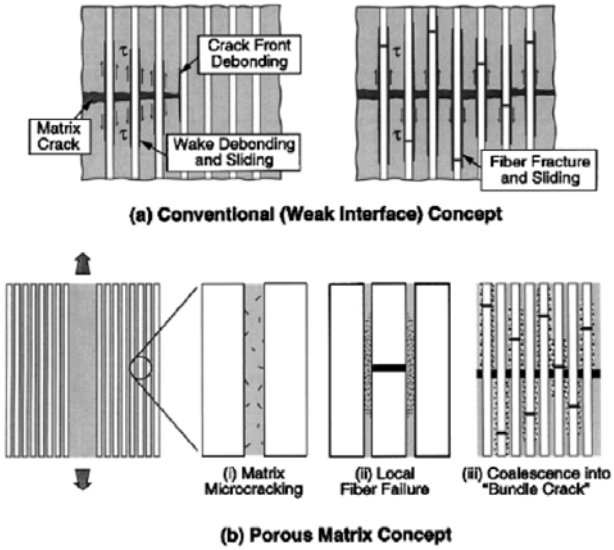

Figure 2. Damage tolerance processes in (a.) conventional dense-matrix weak interface CFCCs and (b.) porous matrix CFCCs without fiber coatings [29]. Figure reproduced with permission from John Wiley & Sons, Inc.

A weak fiber/matrix interphase allows energy to be dissipated throughout the system and transfers the load from matrix to fiber as stress is increased [16]. The knee, or drastic change in slope at approximately 0.1% strain in Figure 3, highlights this weak interphase. Once the proportional limit of the material is reached, the load is transferred from matrix to fiber and continues to perform under higher loads [29].

The oxide fibers and oxide matrices within oxide/oxide materials bond very strongly with each other, creating such a strong fiber/matrix interphase that fiber coatings are unable to be applied after fabrication. Oxide/Oxide CMCs are resultantly designed with weak and porous matrices, approximately composed of 25% air, that gradually fail under load and allow for the load to be continuously transferred from matrix to

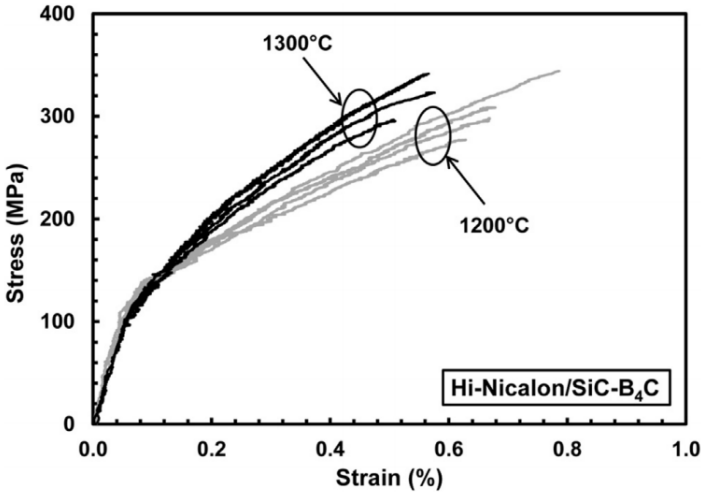

Figure 3. Tensile stress-strain curve obtained for Hi-Nicalon^{TM}/SiC-B_4 (Advanced SiC/SiC) Ceramic Composite at 1200°C and 1300°C [22]

fiber. This continuous load transfer or load sharing is shown in Figure 4 and is the reason for a relatively linear stress-strain relationship to failure [16].

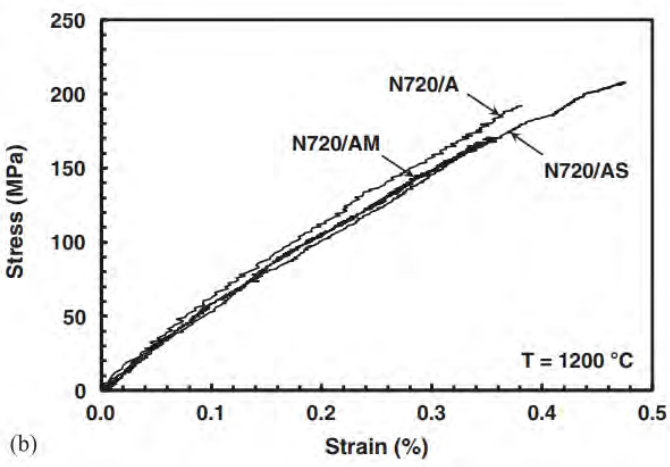

Figure 4. Tensile stress-strain curves obtained in tests conducted at 0.05 mm/s in laboratory air for N720/A, N720/AS, and N720/AM ceramic composites at 1200°C [16]

SiC/SiC composites are Non- Ox/Ox CMCs able to withstand temperatures higher than 1200°C however, they are incredibly expensive materials. Although their weak fiber/matrix interphase allows for the application of fiber coatings and makes them somewhat oxidation resistant, their ability to operate above 1200°C is an unnecessary

quality in turbine engine applications and their high cost renders them an unattractive option. Ox/Ox materials are able to operate in temperatures working up to 1200°C and are significantly cheaper to manufacture than SiC/SiC composites.

Oxide/Oxide materials are oxidation resistant but have several other limitations in high-temperature environments. Previous research efforts reveal Ox/Ox materials severely degrade in high-temperature, steam environments due to loss of matrix porosity and depletion of the mullite (Sl_2O_3) phase within the Nextel^{TM} 720 fiber. When undergoing creep loading in a steam environment the porous matrix undergoes a rapid densification, preventing a continuous load transfer from matrix to fiber and resulting in premature failure. In addition, the mullite contained in the outer 2 micrometers of the 12 micrometer diameter fiber reacts during loading and is depleted from the material, reducing the load-carrying diameter of the fiber from 12 micrometers to 8 micrometers. Although it combats oxidation, the material still has various limitations that must be considered [16].

2.3 Nextel^{TM} 720/Alumina and Nextel^{TM} 720/Alumina-Mullite CMCs

Nextel^{TM} 720/Alumina (N720/A) is a ceramic matrix composite material composed of Nextel^{TM} oxide fibers and an alumina oxide matrix. Nextel^{TM} 720/Alumina-Mullite (N720/AM) is a ceramic matrix composite material composed of Nextel^{TM} oxide fibers and an alumina-mullite oxide matrix. Nextel^{TM} fibers are made by The 3M^{TM} Company in Maplewood, MN, and the composite is fabricated by COI Ceramics in San Diego, CA. The operating temperatures for these CMCs range from 0°C to 1200°C. Figure 5 highlights the changes in material properties for Nextel 720/A specifically, at 23°C and 1200°C. Results show that as temperature increases, the ultimate tensile strength of the material sees minimal change, along with modulus of elasticity and percentage strain prior to failure. These results mirror the characteristic

material properties of a ceramic matrix composite.

CMC system	Temperature (°C)	UTS (MPa)	Modulus (GPa)	Strain (%)	PL (MPa)
Nextel720/A	23	144	69	0.24	80
Nextel720/A	1200	140	55	0.30	35

Figure 5. Material Properties of Experimental Materials as a function of Temperature [1]

The Nextel^{TM} 720 fiber comes from the Nextel^{TM} family of oxide fibers manufactured by The 3M^{TM} Company. These fibers were designed for a variety of high temperature industrial and structural applications. Specifically, the Nextel^{TM} 610 and 720 fibers were designed to carry heavy structural loads and used in materials with metal, ceramic, or polymer matrices. According to 3M^{TM}, the 720 fiber was designed for use in ceramic matrix composites because of its high creep resistance and retaining of strength properties at elevated temperatures. Figure 6 shows the single filament tensile strength of the 720 and various other Nextel^{TM} fibers. The 720 fiber strength value measured is approximately 2000 MPa. Figure 7 illustrates the 720's high strength retention at temperature. This material's ability to maintain strength properties from 20°C to 1200°C is outstanding and validates its use in high-temperature applications. 3M^{TM} attributes this property to reduced grain boundary sliding which prevents grain growth under thermal load [1].

Nextel^{TM} 720 fibers have a diameter of 8 to 14 microns and they are woven and laid in the 0°C and 90°C directions prior to bonding. After eight or so plies are laid up in a preform, the material undergoes slurry infiltration, pressureless sintering, and is baked in an oven at elevated temperature [4]. Prolonged exposure to environmental temperatures greater than 1200°C will lead to a decrease in material performance and catastrophic failure. N720/A and N720/AM rely on their porous matrices for crack deflection, as do all oxide/oxide CMCs [16]. These materials do not have fiber coatings

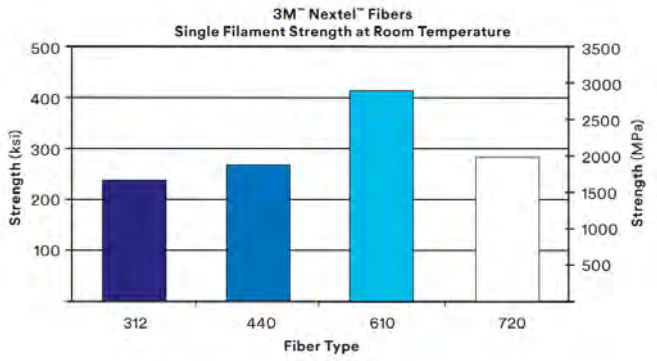

Figure 6. 3M^{TM} single filament strength testing data of Nextel^{TM} series fibers [1]

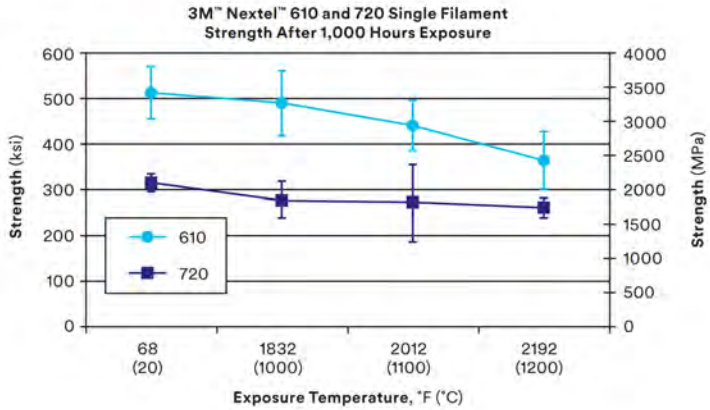

Figure 7. 3M^{TM} creep testing data of Nextel^{TM} series fibers [1]

nor show evidence of interphase between the fibers and the matrix post-processing; it is synthesized using the sol-gel method [28]. The Nextel 720 fibers within N720/A and N720/AM have a chemical composition of 85 wt.% Al_2O_3 and 15 wt.% SiO_2 [1].

The alumina matrix of N720/A is greater than 99% Al_2O_3. The N720/A panel used to process test specimens contains twelve 0°/90° woven plies and has an average density of approximately 2.74 g/cm^3, a matrix porosity of approximately 24.3%, and a fiber volume of approximately 45%. The alumina-mullite matrix of N720/AM has a matrix porosity of approximately 24.0%, a fiber volume of approximately 45% and the panel has an average density of 2.77 g/cm^3 [19].

2.4 Cusil Active Brazing Alloy (Cusil-ABA®)

If ceramic matrix composites are to replace conventional alloys in aerospace systems, it is imperative that they are able to be formed into more complex geometric shapes. Material fabrication processes inherently limit the design complexity of a specific part. Many metal parts are created by taking bulk material and machining it down into smaller pieces while additively manufactured materials are extruded or "printed" into existence from the ground-up. Regardless of the material and manufacturing process, restrictions such as cost, size, and weight limit the parts that can be created in a singular effort. These design restrictions are especially applicable in aerospace where large vehicles and intricate systems such as aircraft turbine engines require geometrically complex parts made from technologically advanced materials. Manufacturing smaller components that can be joined together to form larger parts is a method aerospace companies are exploring to overcome these design restrictions.

To achieve a more geometrically complex part, ceramic matrix composite materials may need to be joined together with other composites or integrated with high-temperature metals and alloys already present in the system. Although there are a variety of joining methods researchers have looked into such as glass-ceramic bonding, diffusion bonding, and transient eutectic phase bonding, the joining method of brazing has become a common method used by researchers because of its minimal cost, efficacy, and application potential [3].

Brazing is the process of joining two dissimilar metals together by using a filler metal, or braze. It is used to create nonstandard configurations or more complex geometric shapes as opposed to welding which is used more for connecting or patching smaller, localized areas. A general schematic of the "braze sandwich" used for this research effort can be seen in Figure 8. Instead of welding which would only join the outer edges of two Nextel™ 720/A specimens, a braze foil can be cut to size and

placed in between the specimens, greatly increasing the surface area of the bond and providing greater flexibility for "sandwich" designs. For this research effort, the braze foil used was Cusil Active Brazing Alloy (Cusil-ABA®).

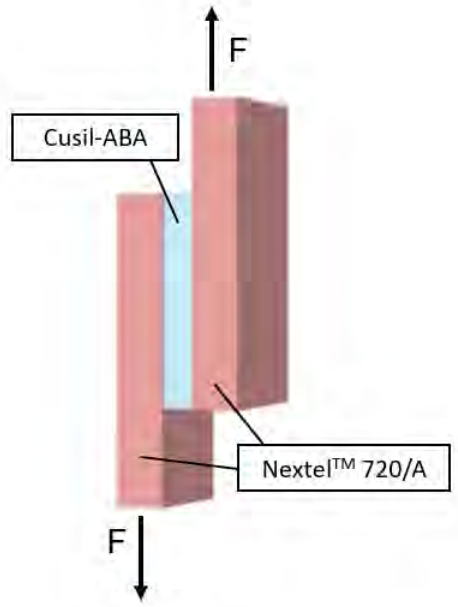

Figure 8. Schematic of joined specimens

Brazing's ability to create a waterproof and airtight continuous seal between composites, metals, or any combination of the two, offers great flexibility in comparison to other joining processes. Wettability and infiltration are two very important properties when attempting to join dissimilar materials. Although there are no universal standards of measurement for these properties, they are incredibly important for characterizing a brazed joint. Wettability describes a open pore material's ability to allow braze spreading on its surface and capillary penetration of braze into its structure. Infiltration characterizes the flow of braze into the braze material and away from the brazing surface. It is important that a braze exhibits adequate wetting and adherence to the base materials. In addition to its joining abilities, the braze must continue to perform after adherence. Brazes must demonstrate resistance to creep and oxidation,

contain a coefficient of thermal expansion similar to that of the joined materials, and have a high thermal conductivity. It is desired for the braze of the material to have a higher liquidis temperature than the materials being brazed [3][14].

The specimens used for this research effort were brazed by Morgan Advanced Materials, Wesgo Metals, in Hayward, CA. The specimen geometry of a brazed sample is defined in Chapter 3. The company was able to take two Nextel^{TM} 720/A specimens and assemble them together using their Cusil Active Brazing Alloy (Cusil-ABA®). The Cusil-ABA® is a member of the Morgan Advanced Materials, Active Brazing Alloys family. These specific types of brazing materials contain active components that promote wetting on ceramic surfaces and allow the braze to wet and bond to almost any metallic or composite surface. Unlike conventional brazing techniques, this process allows for vacuum-tight ceramic-to-ceramic bonding without using practices that could damage the material such as metallizing, firing, and electroplating. The Cusil-ABA® is 63% Silver (Ag), 35.25% Copper (Cu), and 1.75% Titanium (Ti). The titanium present in this braze acts as a reactive filler metal and facilitates chemical reactions at the ceramic's surface, resulting in promoted braze wettability and flow characteristics [3]. Research has shown that active brazing alloys containing Ti produce strong joints with desirable microstructural qualities [25]. This research effort conducted microstructural characterization of the brazed joint to determine the joint's strength and observe the bond strength between the Nextel^{TM} 720/A CMC and Cusil-ABA® braze. Specific material properties of the Morgan Advanced Materials Cusil-ABA® braze are found in Figure 9 [10].

Although brazing provides a more complex geometry, the addition of a foreign material can limit the a specimen's tensile strength, creep resistance, shear strength, or other performance metric. For this research effort, it is known that the braze used by Morgan Advanced Materials limits the single-lap-joint brazed specimen's

Liquidus Temperature	815 °C
	1500 °F
Solidus Temperature	780 °C
	1435 °F
Coefficient of Thermal Expansion (CTE)	18.5 x 10^{-6}/C, for 20 – 500 °C
	10.3 x 10^{-6}/°F, for 68 – 932 °F
Thermal Conductivity (Calculated)	180 W/m·K
	104 BTU/ft·h· °F
Density	9.8 Mg/m^3
	0.354 lb/in^3
Yield Strength (0.2% offset)	271 MPa
	39.9 x 10^3 lb/in^2
Tensile Strength	346 MPa
	50.2 x 10^3 lb/in^2
Elongation (2in/50mm gage section)	20%
Electrical Resistivity	44 x 10^{-9} ohm·m
Electrical Conductivity	23 x 10^6/ohm·m
Vapor Pressure (Calculated)	
Recommended Brazing Temperatures	830 – 850 °C
Recommended Brazing Atmospheres	10^{-5} mm Hg, inert gas

Figure 9. Specifications for Cusil-ABA® used by Morgan Advanced Materials [10]

allowable operating temperature range. Morgan Advanced Materials claims that this braze can operate in temperatures up to 650°C which is much lower than the 1200°C upper temperature limit of the Nextel^{TM} 720/A. It is important to note that 650°C is 165°C cooler than the braze's liquidis temperature provided in Figure 9.

2.5 Previous Research Efforts

Several AFIT research efforts have looked into the creep and fatigue performance of Nextel^{TM} 720/Alumina. In 2006, Eber [23] was the first to look at high-temperature mechanical behavior of N720/A and thus focused on tension-tension fatigue at a loading frequency of 1.0 Hz and at 1200°C. Eber's work was continued by Hetrick [19] who researched the impact of different loading frequencies, specifically 0.1 Hz and 10.0 Hz, and compared the results to Eber's work at 1200°C. It was found that slower loading frequencies provided the most damage to the material [19]. N720/A is a potential material for aircraft turbine engines. As aircraft engine designers have aimed to improve

thermodynamic efficiency, a need for materials able to withstand higher temperatures has developed. N720/A with effusion holes, small holes drilled into the material to facilitate film cooling, is a potential solution for this application. In 2018, Minor [17] looked into laser-drilled effusion holes on N720/A and their impact on the material's creep performances in air and steam. The study found that localized damage from laser heat translated to a severely degraded creep resistance. This degradation was exacerbated in steam [17]. Harkins [6] continued to look into N720/A creep performance with effusion holes however, used diamond tooling for drilling instead of a laser. The drilling continued to provide localized matrix damage which, in addition to severing load-bearing fibers, also decreased the material's creep resistance. Reduction of creep resistance for diamond-drilled specimens was once again exacerbated in steam [6].

Nextel^{TM} 720/Alumina-Mullite was creep tested by Genelin [5] in 2008. Genelin worked in air, steam, and argon environments at 1200°C with 0°/90° fiber oriented material. Genelin reported that a steam environment was more detrimental to creep performance than others and that the composite showed primary and secondary creep regimes for each environment [5]. Creep testing was continued in 2010 by Ozer [15] and Kutsal [9]. Both researchers focused on creep, Ozer looked at 45°/-45°fiber orientation panels and Kutsal tested in 1000°C and 1100°C air and steam environments. Both efforts found steam to have a detrimental impact on creep performance [15][9]. In 2020, N720/AM was fatigue tested at 1200°C in air and steam by Witzgall [27]. Due to electrical problems and complications from a global pandemic, refined results were gathered in steam but not in air. Testing in air at 1200°C needed to be repeated in order to completely and accurately characterize the material's fatigue behavior. Procedures used by Witzgall [27] were replicated for this research effort.

Prior research teams used gathered data to create a variety of plots, characterizing

material behavior. These curves/graphs include: (a) S-N, (b) Stress Hysteresis, (c) Normalized Modulus, (d) Strain vs. Cycle, and (e) Retained Tensile Strength. "S-N" curves illustrate the relationship between the maximum fatigue stress value of a specific test and the number of corresponding cycles it can withstand prior to failure. Stress Hysteresis curves plot stress versus strain values for individual cycles to determine strain accumulation as stress and cycle count are increased. Normalized modulus curves identify a material's stiffness and how it changes with cyclic loading. By calculating the modulus of elasticity for every cycle and subsequently dividing those figures by the first or second cycle modulus value, normalized modulus values are created and plotted versus cycle count. If the normalized modulus value decreases as cycle count increases, then the material loses stiffness with cycling; the opposite is true if the modulus value increases. A strain versus cycle plot depicts the change in accumulated strain as a function of cycle count and a retained tensile strength bar chart shows the ultimate tensile strength (UTS) value of a fatigued specimen after surviving a certain number of cycles in comparison to the UTS of an un-fatigued, virgin specimen.

Past AFIT research efforts have found creep to be more damaging to this material's life span than other loading methods and furthermore, the presence of steam in the test chamber rapidly decreases the time and loading necessary for material failure [16]. Materials undergoing sustained loading, particularly in high-temperature steam environments, exhibit accelerated failure [18]. Figure 10 shows the difference in creep strain as a function of time for 80, 100, 125, and 154 MPa creep loads. These results are of unbrazed N720/A specimens in 1200°C air and steam environments.

No previous research has been performed for single-lap-joint brazed CMC specimens. This research effort was intended to be a pilot study for future AFIT research efforts.

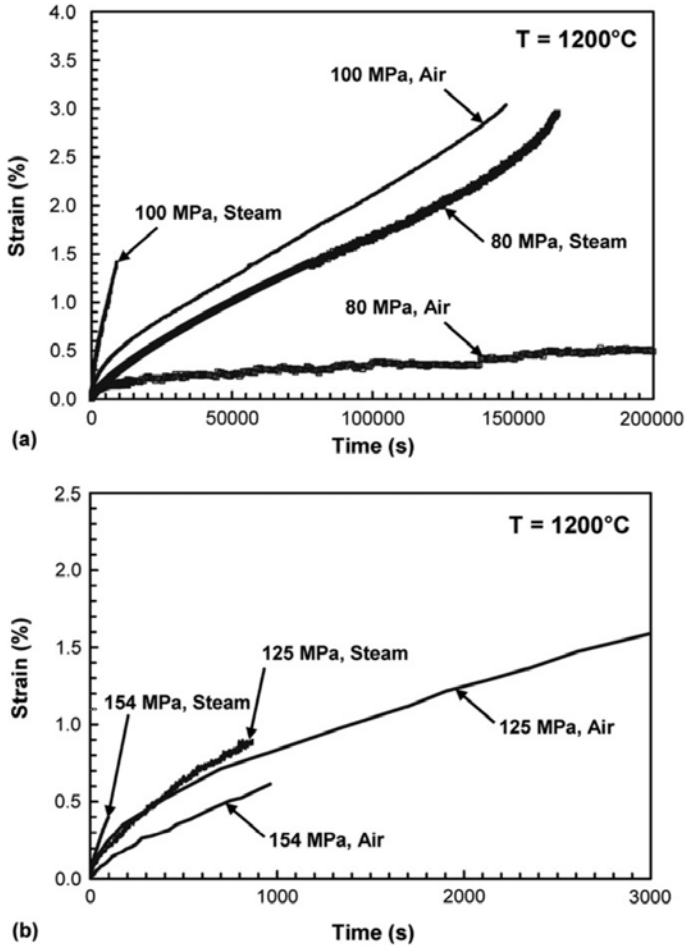

Figure 10. Creep strain v. time for N720/A CMC at 1200°C in air/steam environment: (a.) 80 and 100 MPa, (b.) 125 and 154 MPa [23]

2.6 Thesis Objectives

The objectives of the present study are multifold. The first objective is to assess the effects of incorporating mullite in the matrix material on the mechanical performance and environmental durability of the CMC reinforced with Nextel 720 fibers. The composite studied is the N720/AM ceramic matrix composite consisting of an alumina-mullite matrix reinforced with alumina-mullite Nextel^{TM} 720 fibers. This particular CMC is in many ways similar to the N720/A composite and is also being considered for numerous advanced aerospace applications. This research effort inves-

tigates tension-tension fatigue performance of the N720/AM composite in ambient air at its maximum use temperature of 1200°C. The results are compared and contrasted with those previously obtained for the CMC with the pure alumina matrix. This work complements prior research efforts performed at AFIT that focused on creep performance of this material at 1200°C in air and in steam and on its tension-tension fatigue performance at 1200°C in steam [16][27].

The second objective is to evaluate the effects of an array of small effusion holes on the fatigue performance of the N720/A CMC consisting of the pure alumina matrix reinforced with alumina-mullite Nextel^{TM} 720 fibers. Test specimens contain an array of 17 effusion holes of 0.5-mm diameter. The effusion holes were drilled through the specimen thickness normal to the specimen surface using diamond tooling. Specimens are tested in tension-tension fatigue in laboratory air and in steam environment at 1200°C. The present effort builds on previous AFIT research efforts which investigated the effects of diamond-drilled and laser-drilled effusion holes on creep behavior of this material at 1200°C in air and in steam [6][13]. Specimen fracture surfaces are examined. Damage and failure mechanisms are considered.

In addition, this research effort aims to explore the feasibility of brazing as a technique to join simple CMC shapes to produce a more complex shape. Before this technique is used to produce parts for use in aerospace structural applications, structural integrity and long-term environmental durability of the CMC brazed joints must be assured. This effort characterized tensile strength of N720/A CMC specimens containing a brazed joint at temperatures ranging from 23°to 650°C in laboratory air.

III. Research Methodology

3.1 Chapter Overview

This chapter discusses the laboratory equipment used to complete this research effort and the corresponding procedures. It describes specific dimensions and fabrication details of the test specimens, the temperature calibration process, fatigue testing procedures, and microstructural characterization procedures.

3.2 Mechanical Testing Equipment

Mechanical testing for this research effort was conducted using two different 810 Material Test System (MTS) stations. A 5-kip MTS machine with an integrated steam generator was used to conduct N720/A air and steam fatigue testing as well as tension to failure testing of the brazed specimens. The 5-kip load frame had access to a steam generator and utilized a furnace with a chamber size large enough to house a susceptor, therefore making steam testing possible. A 22-kip MTS machine was used for N720/AM fatigue testing in air.

3.2.1 5-Kip Material Test System Setup

Mechanical testing of N720/A specimens in tension-tension fatigue as well as tension testing of N720/A specimens containing a brazed joint was conducted using a 5-kip 810 Material Test System (MTS) machine. This is a servo-hydraulic testing machine equipped with water-cooled hydraulic wedge grips. This machine is capable of applying a 5-kip tensile load. For all tests on this load frame, the grip pressure was set to 8 MPa. The grips were cooled during testing using a Thermo Scientific Accel 250 Liquid Cooling system with deionized chilled water at 18°C.

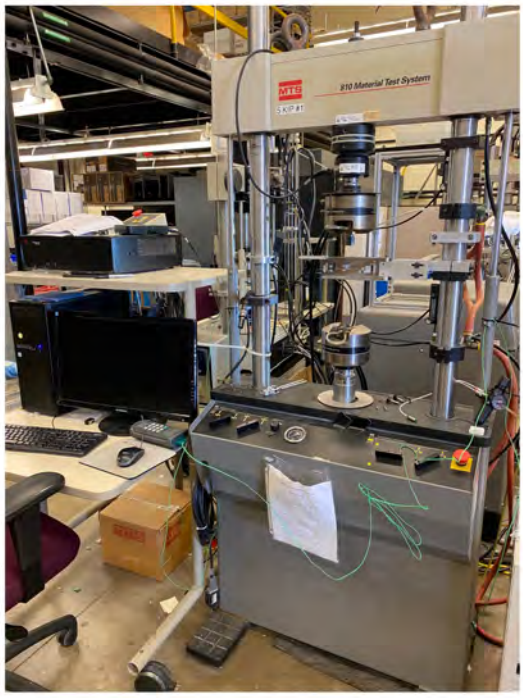

Figure 11. 5-Kip 810 Material Test System

An MTS FlexTest 40 digital controller was used for input signal generation and data collection. Test procedures were programmed using MTS MultiPurpose TestWare® which communicates directly with the MTS FlexTest 40 digital controller [27].

Test procedures are used to set the thermo-mechanical loading history as well as to prescribe the details of data acquisition. In addition, this software permits the setting of failure detectors. More specifically, the failure detectors can be customized by the operator to meet the requirements of each type of test and material. Correct programming of failure detectors permits an automatic shut-down of the test and the testing system once specimen failure occurs.

An AMTECO HRFS-2Z-2700 furnace and a dedicated temperature controller were used to generate a high-temperature environment in the test chamber. Due to the exploratory nature of this research effort, there was a need to characterize material behavior at a variety of temperatures in the vicinity of 650°C as well as at temper-

Figure 12. Thermo Scientific Accel 250 LC, Chiller used to regulate grip temperature

atures reaching 1200°C. The furnace was controlled by an AMTECO temperature controller with two EUROTHERM 2216e digital modules, communicating with the top and bottom furnace elements, respectively. The AMTECO furnace uses Rescor 310M ceramic foam insulation. The test chamber is large enough to fit a susceptor used to achieve a more uniform heating of the test specimen in all high-temperature tests and to contain steam when testing in steam. Figure 13 shows the furnace operating at 1500°C during troubleshooting. Figure 14 shows the AMTECO two-zone temperature controller.

An alumina susceptor was used in all high-temperature tests. The susceptor is an alumina tube with end caps that fit inside the AMTECO furnace. The specimen is inserted through the slots in the susceptor, such that the gage section of the specimen is fully enclosed in the susceptor. The front end cap of the susceptor (Figure 15) has openings that are used for the MTS high-temperature extensometer extension rods

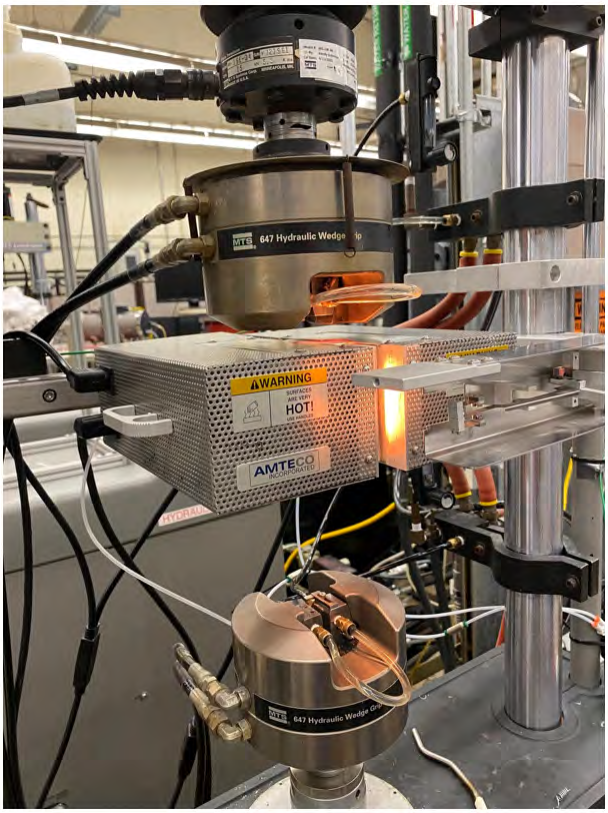

Figure 13. AMTECO Furnace used to create high-temperature environment

Figure 14. AMTECO Two-Zone temperature controller

during fatigue testing or for thermocouples during temperature calibration. The back end cap (Figure 16) has an opening that can be used for the steam feeding tube for fatigue testing in steam. As mentioned above, the alumina susceptor contains highly corrosive high-temperature steam during testing in steam. Furthermore, the use of the alumina susceptor facilitates a more uniform heating of the specimen gage section during all high-temperature tests.

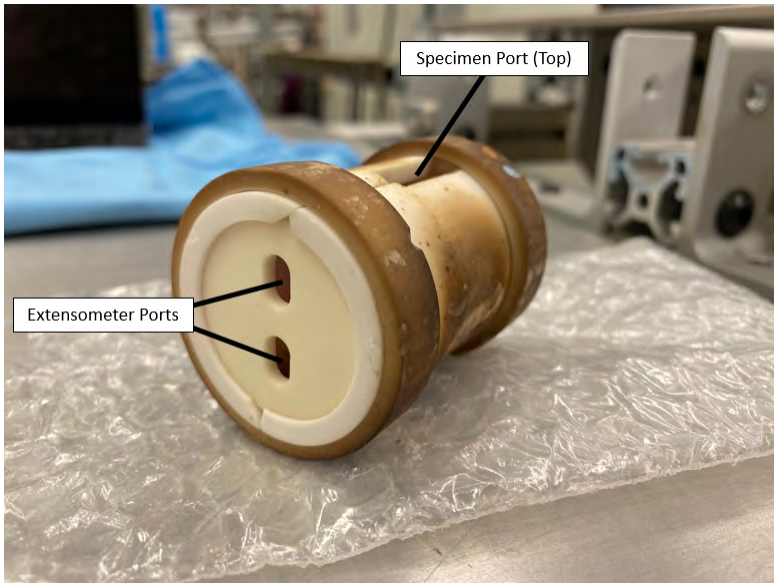

Figure 15. Ceramic Susceptor (Front)

An MTS low-contact force high-temperature extensometer Model 632.53E-14 (Figure 17) was used to measure strain in all tests.

For testing in steam, an AMTECO HRFS-STMGEN steam generator with a Chromalox 2110 temperature controller and deionized water were used to generate steam delivered to the susceptor via the feeding tube. Figure 18 shows the AMTECO steam generator.

3.2.2 22-Kip Material Test System Setup

Mechanical testing of N720/AM specimens was conducted using a 22-kip MTS servo-hydraulic testing machine equipped with water-cooled hydraulic wedge grips.

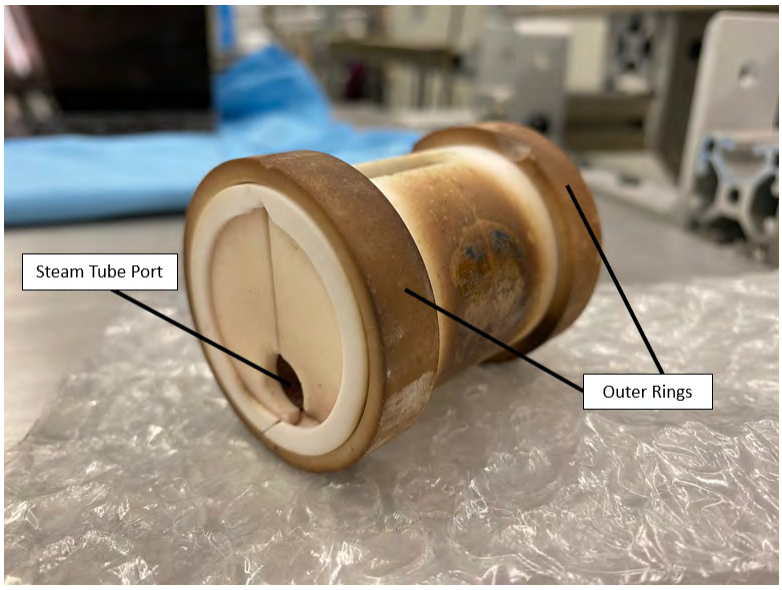

Figure 16. Ceramic Susceptor (Back)

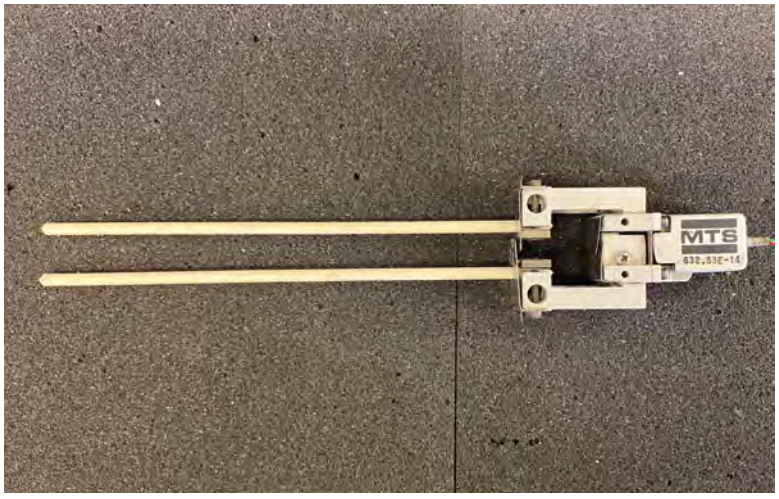

Figure 17. Low-contact force high-temperature MTS extensometer used to measure strain

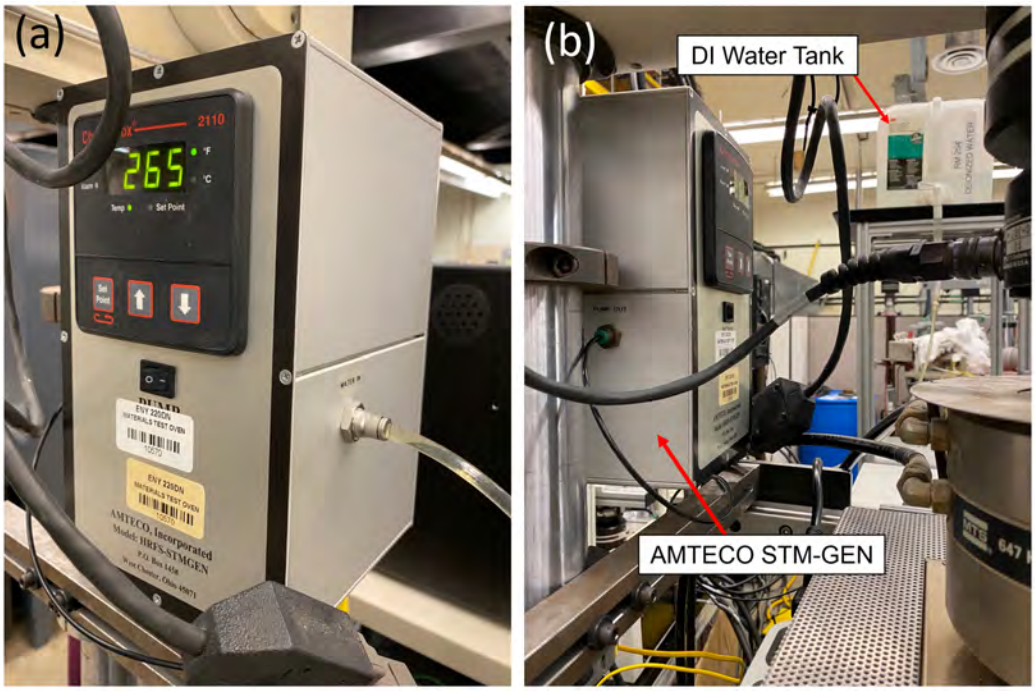

Figure 18. (a) AMTECO HRFS-STMGEN, Steam Generator/Pump, with Chromalox 2110 Temperature Controller, (b) Steam Generator with DI Water Holding Tank and feed tube

This testing system is capable of applying a 22-kip tensile or compressive load. The grip pressure was set to 2.5 MPa for all tests on this station. When testing on the 22-kip machine we utilized the same water chiller, MTS digital controller, MTS MultiPurpose TestWare software and extensometer as those used when testing on the 5-kip machine.

An MTS 653 furnace (Figure 20) was used to heat the test specimen to 1200°C. This furnace was controlled by an MTS Temperature Controller with two EUROTHERM 2216e digital modules, communicating with the left and right heating elements. This two-zone MTS furnace uses Rescor 310M ceramic foam insulation. This furnace is not large enough to house a susceptor and therefore was only used for testing in laboratory air.

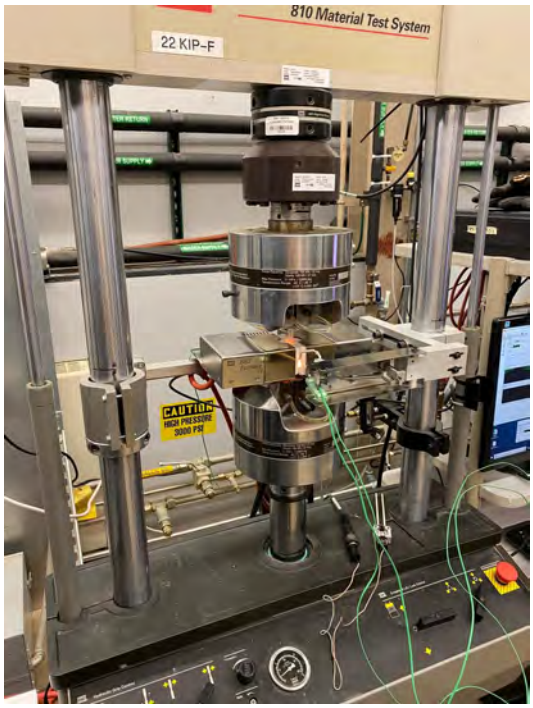

Figure 19. 22-Kip 810 Material Test System

Figure 20. MTS 653 Furnace

3.2.3 Microstructural Characterization

All tested specimens were examined with the ZEISS SteREO Discovery.V12 optical microscope (Figure 21) equipped with an AxioCamHRc digital camera and AxioVision (Version 4.8) software.

Figure 21. ZEISS Optical Microscope

3.3 Procedures

This section discusses the techniques and procedures used for this research effort. Included are procedures used to fabricate and test the N720/A tensile specimens with effusion holes, the N720/AM tensile specimens, and N720/A specimens containing a brazed joint.

3.3.1 Material and Test Specimen Fabrication

The N720/A composite consists of Nextel^{TM} 720 fibers in a porous alumina matrix and was supplied in a form of a 2.8 mm thick plate. The plate comprised 12 0°/90° woven plies, with a density of ∼2.73 g/cm^3 and a fiber volume of approximately 44%. The composite has no fiber coating and relies on porous matrix for flaw tolerance. A sol-gel process was used to infiltrate the fiber fabric with the matrix. Composite was first dried with a "vacuum bag" technique under low pressure and low temperature, then pressureless sintered [8]. Matrix porosity was ∼25.2%. Micrographs in Figure 22 show the as-processed composite microstructure of the untested, as-received material.

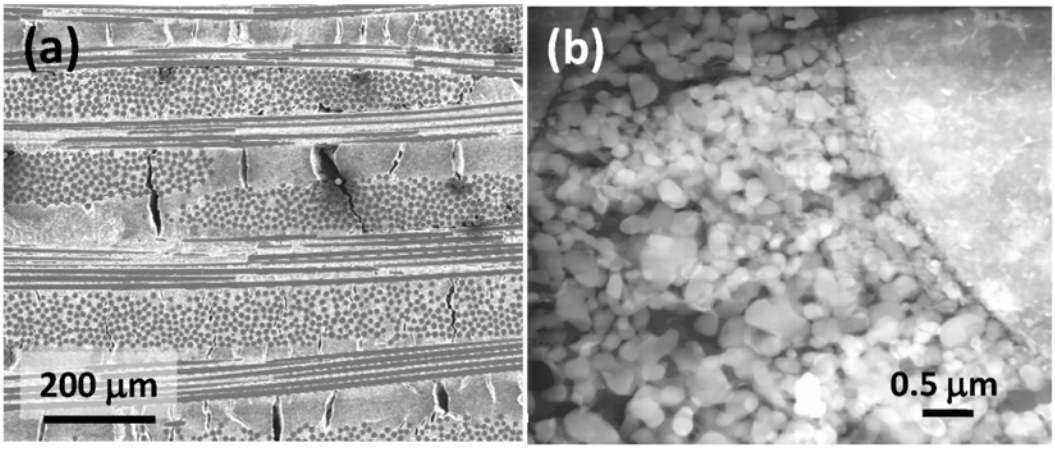

Figure 22. SEM micrographs of the as-processed N720/A composite showing: (a) microstructure overview, (b) porous nature of the matrix. Reproduced from [17].

The N720/AM composite consists of Nextel^{TM} 720 fibers and a porous matrix composed of mullite and alumina particles in a sol-gel derived alumina. Matrix composition contains approximately 12.5% (by volume) of mullite. The N720/AM composite was supplied in a form of a 3.2 mm thick plate, comprised of 12 0°/90° woven plies. Composite had a density of ∼2.52 g/cm^3 and a fiber volume of $V_f \approx 38.5\%$. Matrix porosity was ∼29.8%. The N720/AM laminate was fabricated following the procedure similar to that used to fabricate the N720/A composite. The composite has no fiber coating and relies on porous matrix for damage tolerance. The overall

microstructure of the N720/AM CMC is presented in Figure 23, which shows 0° and 90° fiber tows as well as numerous matrix cracks. In the case of the as-processed material, most are shrinkage cracks generated during composite synthesis rather than matrix cracks produced during loading.

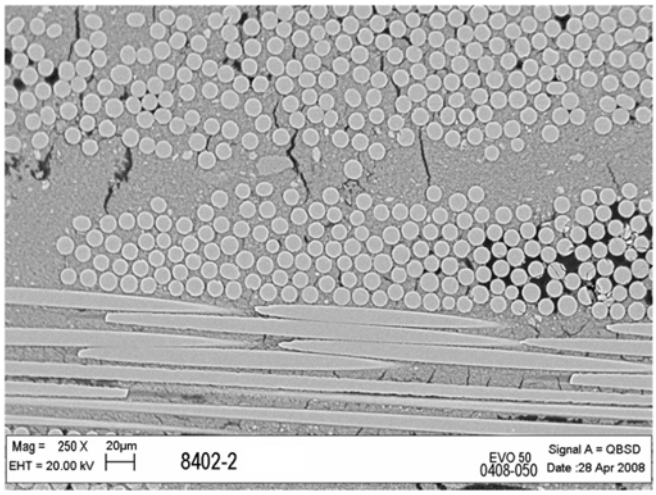

Figure 23. Typical microstructure of the N720/AM ceramic composite. Micrograph courtesy of A. Szweda, COI Ceramics Inc.

Standard dogbone-shaped specimens were used in all tension-tension fatigue tests. Specimens were cut from the composite panels in the AFIT model and fabrication shop using a water-cooled diamond saw according to the drawing shown in Figure 24 [27]. To evaluate the effects of the effusion holes on the tension-tension fatigue behavior of the N720/A composite, test specimens included an array of 17 holes in the gage section. The effusion holes had a diameter of 0.5 mm and were drilled through the specimen thickness normal to the specimen surface using diamond tooling. Figure 25 shows the drawing of the test specimen containing an array of holes. In the case of the specimens with holes an "effective" cross-sectional area was used to calculate engineering stress. The effective area was calculated as follows: (1) first the volume of the gage section of the unnotched specimen was determined, (2) next the volume removed by drilling of the 17 holes was subtracted from the unnotched

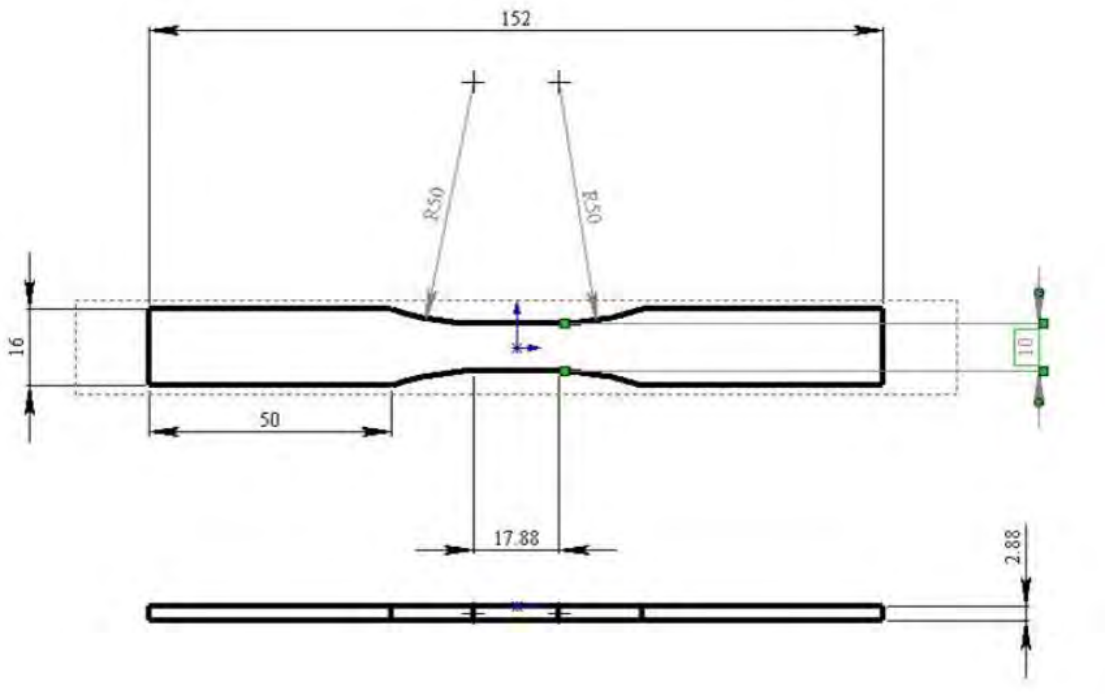

Figure 24. Standard tension-tension fatigue test specimens [27]

volume, (3) finally the result of the subtraction obtained in the previous step was divided by the length of the gage section to obtain the effective cross-sectional area. The effective cross-sectional area of a typical test specimen was 97-98% of the nominal cross-sectional area.

To investigate the feasibility of using brazing as a technique to join CMCs, single-lap-joint brazed N720/A specimens were tested in tension to failure at temperatures ranging from 23° to 650° C in laboratory air. Figure 27 shows a drawing of a single-lap-joint brazed test specimen. A N720/A composite panel was cut into rectangular blanks in the AFIT model and fabrication shop using diamond grinding. The rectangular blanks were then shipped to Morgan Advanced Materials (Hayward, CA) for brazing with Cusil-ABA braze alloy. The first step in the brazing process involved cutting a 0.002-in. thick Cusil-ABA braze alloy to sample width. Next the film of the Cusil-ABA braze alloy was bonded to one side of the CMC blank using a vacuum

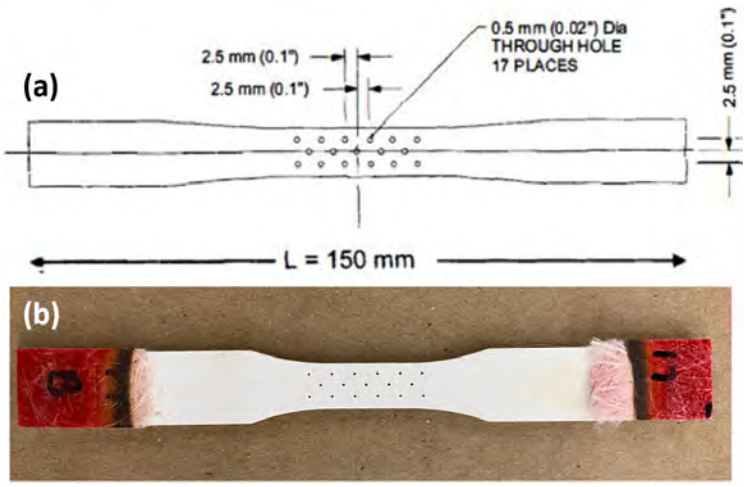

Figure 25. Nextel^{TM} 720/A, fatigue testing specimens with an array of 17 holes: (a) Drawing [6], (b) Test Specimen

compatible braze adhesive.

Simple ceramic tooling was used to align the components of the specimen assembly and a dead weight of approximately 275 g was applied. The bonding of the braze to the CMC specimens followed a very specific procedure. The joint was vacuumed to a pressure near 10e-4 Torr and subsequently heated to 760°C, at a rate of 7°C/min. After being held at 760°C for ten minutes, the assembly was heated to 840°C at a rate of 7°C/min. The assembly was held at 840°C for five to seven minutes before being cooled to 500°C at a rate of 7°C/min, then finally cooled to room temperature [10]. Before testing fiberglass tabs were bonded to the gripping portions of all test specimens to protect the composite and prevent damage from the wedge grips. All tabs were bonded using the M-Bond 200 adhesive [12]. In the case of the fatigue test specimens, fiberglass tabs were 1 mm thick.

Preparation of single-lap-joint brazed test specimens required the use of 3 mm thick aluminum alloy tabs along with the 1 mm thick fiberglass tabs. To ensure that tensile loading was applied along the centerline of the specimen, 3 mm thick aluminum alloy tabs were bonded to the inner faces and 1 mm thick fiberglass tabs, to the outer faces of the specimen gripping sections. All tabs were bonded using the

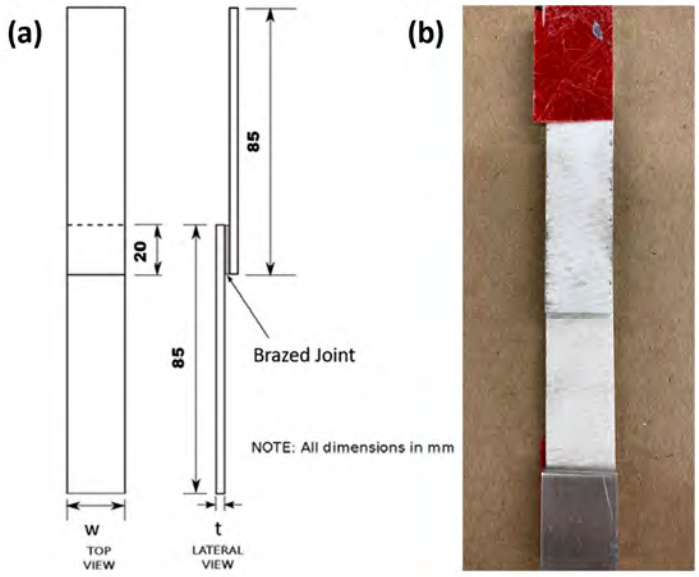

Figure 26. Nextel^{TM} 720/A single-lap-joint brazed test specimen: (a) Drawing [6], (b) Test Specimen

M-Bond 200 adhesive. A single-lap-joint brazed test specimen with tabs prepared for temperature calibration is shown in Figure 27.

3.3.2 Temperature Calibration

Temperature calibration was performed using the same process for all materials. For each material, an extra specimen was set aside specifically for calibration purposes. Thermocouples were placed on opposite sides of the gauge section and enclosed by small rectangular pieces of scrap CMC material. These small tiles had indentations on their inner side to cover the thermocouple leads and create a flush fitting with the specimen; this also created a flat surface for wiring. The scrap material, thermocouples, and calibration specimen were wrapped in piano wire to secure the materials together, seen in Figure 28. Calibration specimens used on the 5-kip machine used a ceramic specimen susceptor while those on the 22-kip machine did not.

For specimens tested on the 5-kip machine, thermocouple wires were fed through the extensometer port of the specimen susceptor prior to being wrapped in piano wire.

This ensured that thermocouple wires could be connected to thermometer ports once in the furnace. This also prevented the wires used to secure the scrap CMC material from coming into contact with thermocouple wires and creating a short circuit. Once wrapped, these specimens were fitted into the ceramic susceptor and enclosed, as seen in Figure 27.

Because temperatures within a furnace may vary from temperatures output by the temperature controller and those read on the Eurotherm, an Omega HH501BR thermometer was connected to the thermocouple terminals to obtain accurate temperature recordings from the specimen's surface. The presence of a specimen susceptor is another variable which may alter the specimen's experienced temperature.

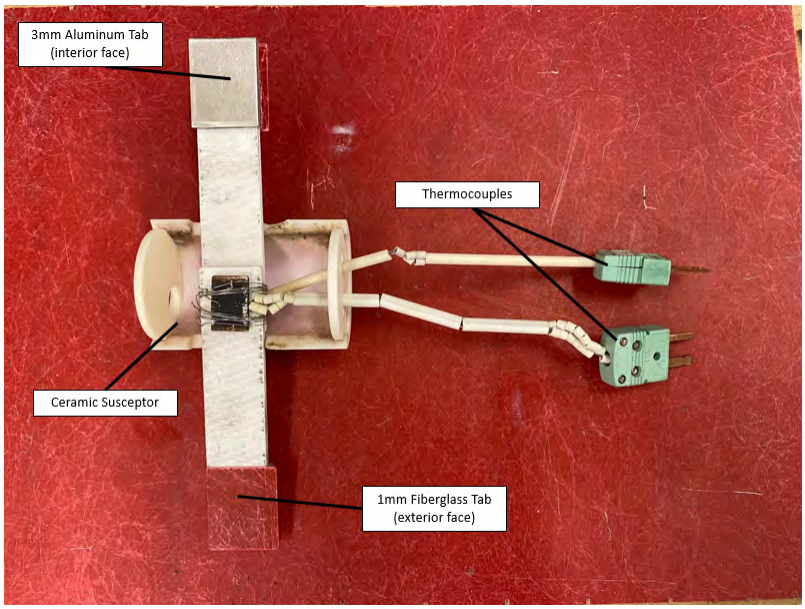

Figure 27. Tabbed specimen prepped for temperature calibration

Calibration of each furnace was completed in two phases. The first phase involved a slow increase in furnace temperature set points until the temperature output on the thermometer matched the desired test temperature. For tests reaching 650°C, for example, the temperature of the furnace was increased to 100°C and subsequently increased by 100°C increments up to 300°C. It was then increased to 600°C in 25°C

increments. The final 50°C was reached by adding temperature in 5°C increments. This was a similar process for tests reaching 1200°C, but with larger increments. Adequate dwelling time was allowed in between incremental heating to achieve thermal equilibrium and temperature reading convergence at each step. This ensured the correct specimen temperature was being recorded. For the AMTECO furnace, this process was performed using an MTS procedure. The procedure would continuously ramp the upper and lower elements at 20°C/min unless paused and if so, the furnace would hold that temperature until resumed. This process was repeated until the desired temperature, or average of the upper and lower thermocouple readings, was within 0-5°C of the desired temperature. The AMTECO's upper and lower element temperatures were the same for this entire process; they could not be adjusted to different values manually. For the MTS 653 Furnace, the left and right sides of the furnace were increased by a rate of 25°C/min up to 80% of the desired temperature value. The left and right sides of the furnace were than manually adjusted until the left and right thermocouple readings were within 0-5°C of the desired temperature. Dwelling time at each incremental set point was 10 minutes or greater and final desired set points were recorded.

Once these set points were determined, phase two involved a continuous ramp up to the established set points. As mentioned previously, each furnace had its own temperature ramp rate. During this phase, temperature was increased in the same manner as during testing to ensure that significant over-temping of the material did not occur.

3.3.3 Tension to Failure Tests

Prior to loading, the cross-sectional area of each test specimen was measured and recorded. The measurements of the cross-sectional area were then used to calculate

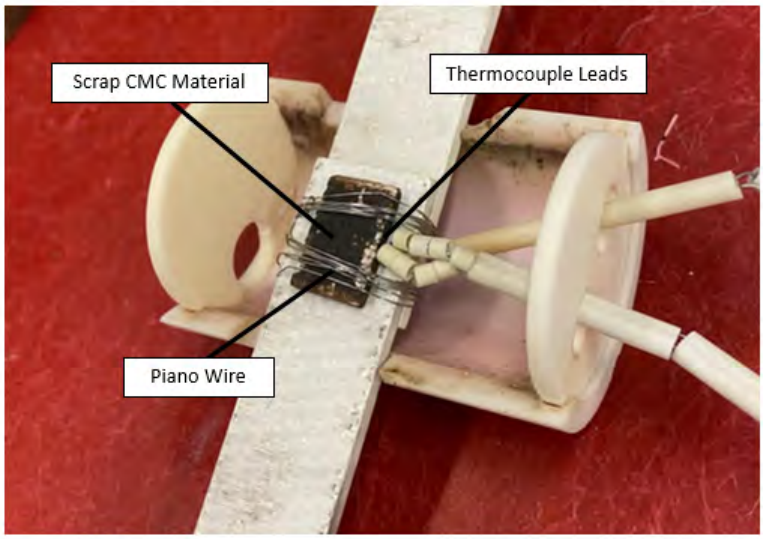

Figure 28. Temperature calibration specimen wiring setup

Figure 29. Omega HH501BR Thermometer used in AMTECO furnace temperature calibration

engineering stress. All tension to failure tests were performed in displacement control at a constant displacement rate. The displacement rate was set to 0.02 mm/s for testing single-lap-joint brazed specimens and to 0.05 mm/s for testing specimens that achieved fatigue runout of 100,000 cycles without failure.

3.3.4 Tension-Tension Fatigue Testing

All fatigue testing was conducted at 1200°C. The test specimen was heated to 1200°C at 20°C/min in tests using the AMTECO two-zone furnace and at 25°C/min in tests using the MTS 653 furnace. Then the specimen was held at test temperature for additional 50 min prior to testing. All fatigue tests were conducted at a frequency of 1.0 Hz with a ratio of minimum to maximum stress R = 0.05 and a sawtooth waveform. Fatigue runout was defined as survival of 100,000 cycles without failure.

3.3.5 Microstructural Characterization

All test specimens were examined with an optical microscope before and after testing. Examination with an SEM was not possible at this time. It is strongly recommended that the tested specimens be examined with an SEM to gain insight into damage and failure mechanisms.

IV. Testing, Results, and Analysis

4.1 Tension-Tension Fatigue Performance of Nextel^{TM} 720/AM Specimens in Air at 1200°C

Tension-tension fatigue testing of N720/AM specimens was performed at 1.0 Hz with a sawtooth waveform. The ratio of the minimum stress to maximum stress was R = 0.05. Fatigue runout was set as 100,000 cycles. Such definition of fatigue runout permits direct comparison of the current study's results with those produced in previous AFIT studies on oxide/oxide CMC fatigue behavior [19][23][27]. It is noteworthy that all N720/AM specimens tested in fatigue in this work failed within the extensometer gage section.

Fatigue testing of N720/AM is summarized in Table 1 where the results of fatigue testing of N720/AM at 1200°C in steam from a prior study [27] are included for comparison. Fatigue tests in this work were performed with the maximum stresses ranging from 100 to 140 MPa. Genelin [5] reported a 1200°C ultimate tensile strength (UTS) for the N720/AM specimens of 153 MPa. The tensile stress-strain curve for the N720/AM composite in air is shown in Figure 30 alongside N720/A (without effusion holes). The added mullite in the N720/AM matrix yields a less ductile material with a lower modulus of elasticity. Results of the tension-tension fatigue tests on N720/AM specimens are also presented in Figure 31 as stress vs cycles to failure (S-N) curves. Results from prior work obtained at 1200°C in steam [27] are included in Figure 31 for comparison.

Results in Table 1 reveal that at 1200°C in laboratory air, the fatigue limit was 140 MPa (91.5 %UTS at 1200°C). As previously mentioned, this fatigue limit is based on a runout condition of 100,000 cycles which approximates the number of loading cycles expected in aerospace applications at 1200°C. It is recognized that a more

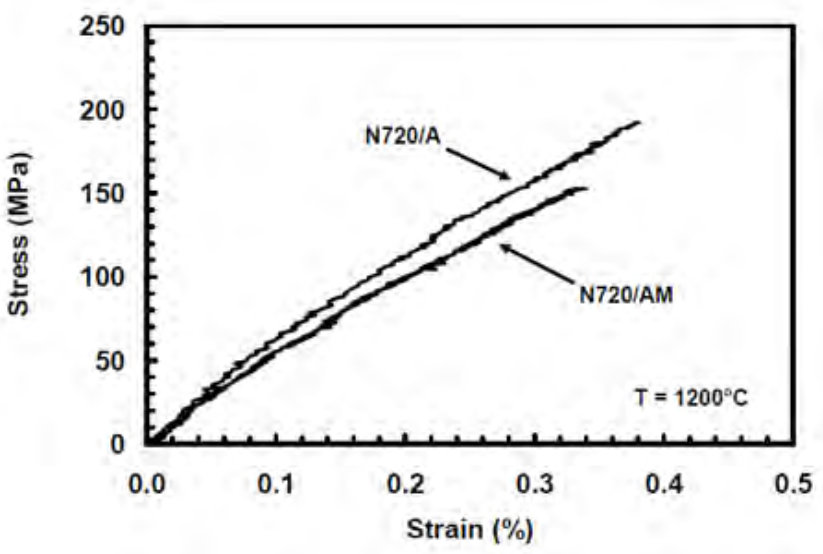

Figure 30. Tensile stress-strain curve at 1200°C for N720/AM composite and N720/A composite without an array of holes [5]

rigorous runout condition would have produced a lower fatigue limit. Steam caused a noticeable deterioration in fatigue performance at 1200°C. As seen in Table 1, the fatigue limit in steam was 120 MPa (78 %UTS at 1200°C). Also seen in Table 1, an increase in maximum stress to 136 MPa resulted in significant degradation of the fatigue performance in steam. The specimen tested in steam with $\sigma_{\max} = 136$ MPa survived only 20,212 cycles.

Figure 32 shows the evolution of the stress-strain hysteresis response with cycles for the N720/AM specimens tested at 1200°C in air. The largest strains were typically accumulated during the first cycle indicating that the most damage occurred on the first cycle. Then the hysteresis loops generally stabilized. Results in Figure 32 also reveal that ratchetting was observed for all tests. Similar behavior was reported for the N720/AM specimens tested in tension-tension fatigue at 1200°C in steam [27] as well as for the N720/A composite without effusion holes tested in tension-tension fatigue at 1200°C in air and in steam [23].

Reduction in stiffness (hysteresis modulus determined from the maximum and

Table 1. Summary of fatigue results for N720/AM composite at 1200°C, in laboratory air environment

Test Environment	Maximum Stress (MPa)	Cycles to Failure (N)	Failure Strain (%)
Fatigue at 1.0 Hz			
Laboratory air	100	107,829[a]	0.079[a]
Laboratory air	120	100,000[a]	0.042[a]
Laboratory air	130	100,000[a]	0.083[a]
Laboratory air	140	100,000[a]	0.036[a]
Steam[b]	60	180,000[a]	
Steam[b]	90	100,000[a]	
Steam[b]	92	100,000[a]	
Steam[b]	120	100,000[a]	
Steam[b]	136	20,212	

[a] Runout. Failure of the specimen did not occur when the test was terminated.
[b] Data from Witzgall, 2020[27].

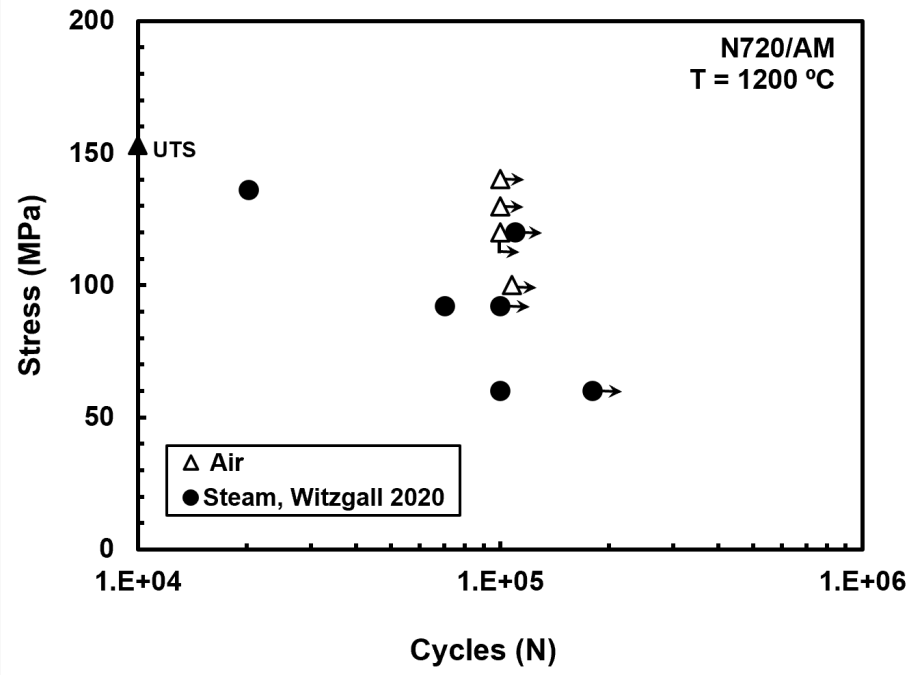

Figure 31. Fatigue S-N curves for Nextel™ 720/AM ceramic composite at 1200°C in air and in steam. Data in steam from Witzgall [27]. Arrow indicates that failure of specimen did not occur when the test was terminated.

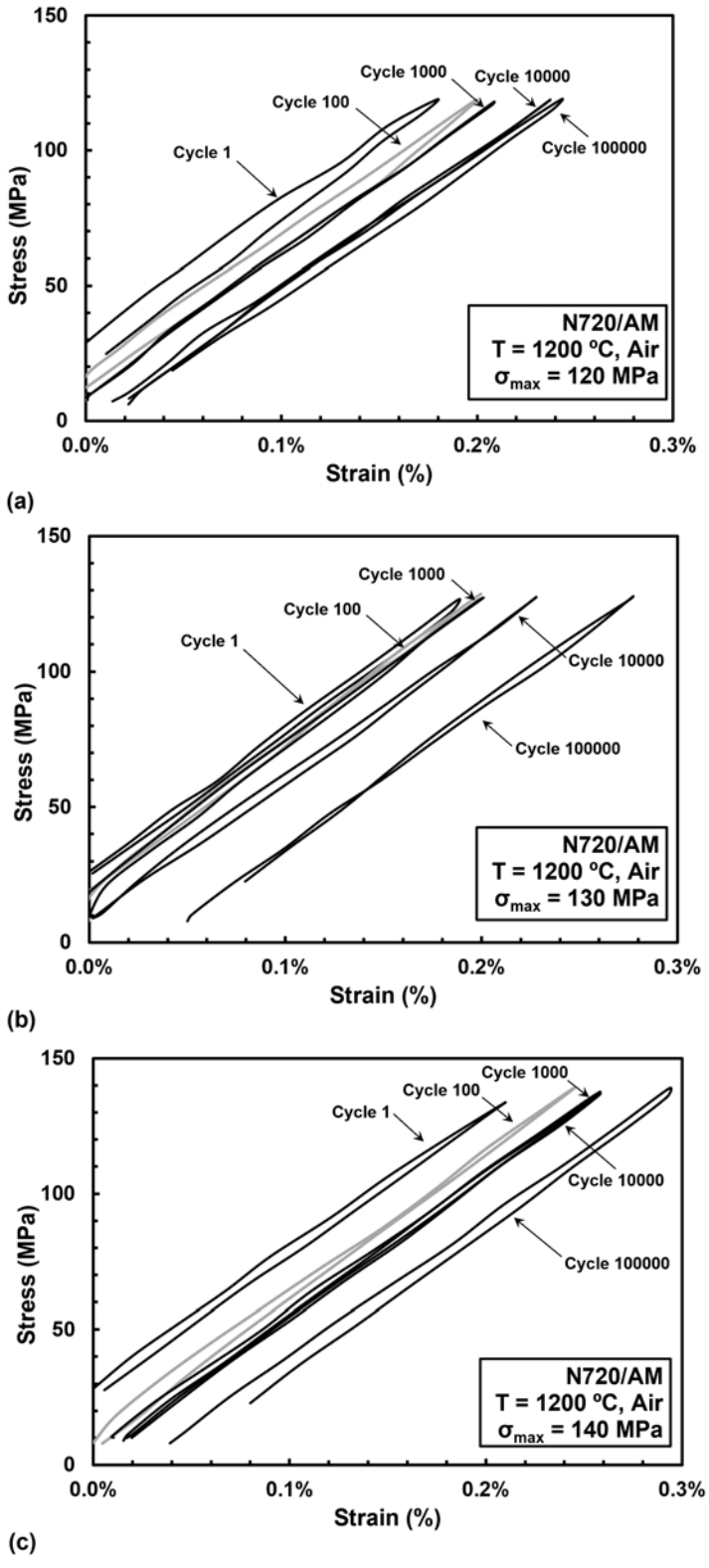

Figure 32. Typical evolution of stress-strain hysteresis response of N720/AM with fatigue cycles at 1200°C in air at: (a) σ_{max} = 120 MPa, (b) σ_{max} = 130 MPa, (c) σ_{max} = 140 MPa.

minimum stress-strain data points during a load cycle) with respect to fatigue cycles reflects the damage evolution during fatigue testing. Change in modulus at 1200°C in air is shown in Figure 33, where normalized modulus (i. e. modulus normalized by the modulus obtained in the first cycle) is plotted vs fatigue cycles. Results in Figure 33 reveal little decrease in normalized modulus with fatigue cycles, indicating that no damage occurred to the load-bearing fibers during 100,000 fatigue cycles. Evidently maximum stress levels in these fatigue tests were sufficiently low to limit damage development. Recall that all specimens tested in air achieved fatigue runout of 100,000 cycles. Note that only limited reduction in normalized modulus with cycles was observed at 1200°C in steam (with the exception of the 136 MPa test that failed early) [27].

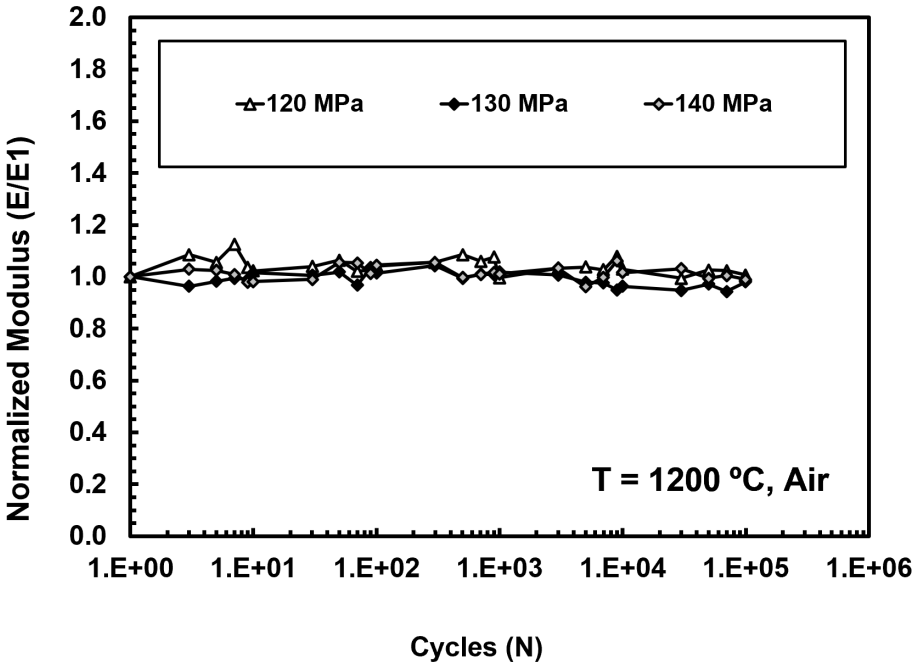

Figure 33. Normalized modulus vs. fatigue cycles for N720/AM in air at 1200°C

Figure 34 shows the strain accumulation with fatigue cycles count for the N720/AM specimens tested at 1200°C for air. Note that all test specimens represented in Figure 34 achieved fatigue runout of 100,000 cycles. Strains accumulated in those tests

were all below 0.083%. Results shown have been adjusted to purely show mechanical strain.

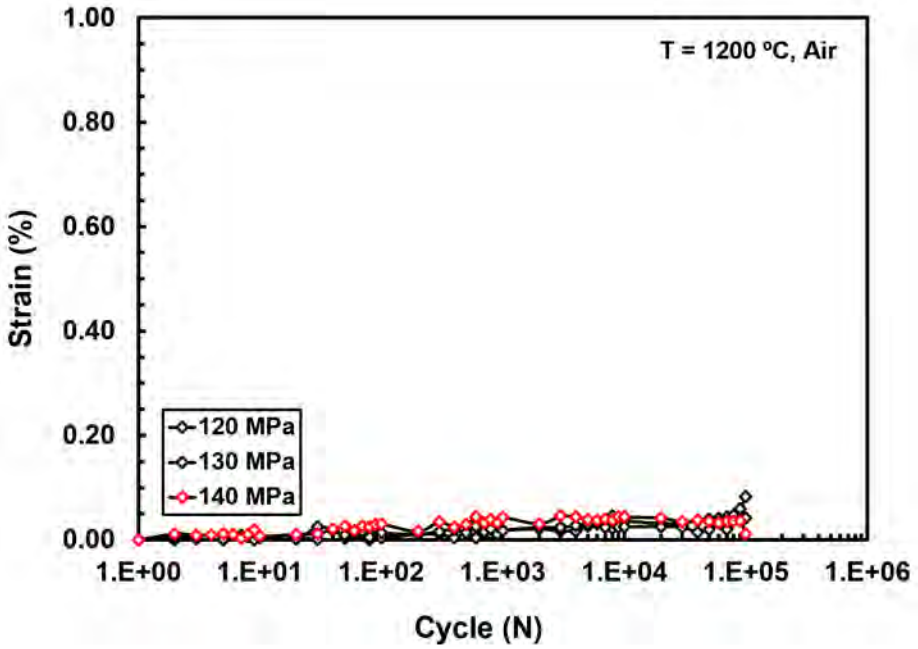

Figure 34. Strain accumulation with fatigue cycles for N720/AM specimens in air at 1200°C

Retained tensile strength of all specimens that achieved fatigue runout of 100,000 cycles was evaluated in tension to failure tests at 1200°C (Figure 35). Evaluation of retained tensile strength is helpful in assessing the degree of damage caused to the composite by prior 100,000 fatigue cycles. As seen in Figure 35 all specimens that achieved fatigue runout in air retained 100% of their tensile strength indicating that no damage occurred to the reinforcing fibers. Witzgall [27] reported that the N720/AM specimens previously subjected to fatigue in steam at 1200°C retained at least 90% of their tensile strength. Such limited (10% or less) loss of tensile strength suggests that the fibers incurred little damage during fatigue testing. Notably, similar retention of tensile strength was reported for the N720/A composite with the alumina matrix subjected to prior tension-tension fatigue at 1200°C in air and in steam [19].

The N720/AM specimen tested in tension-tension fatigue in air with a maximum

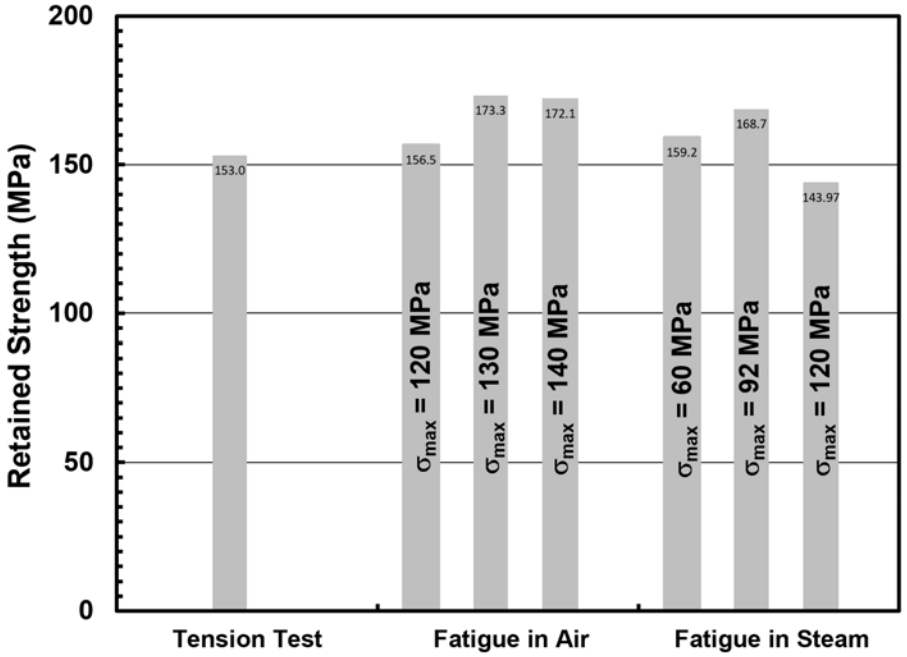

Figure 35. Retained tensile strength of N720/AM specimens subjected to prior fatigue in air at 1200°C. Data in steam from Witzgall [27].

stress of 100 MPa and a cycle count of 107,829 cycles was examined under an optical microscope, seen in Figures 36 and 37. Optical micrographs reveal brushy (or fibrous) fracture with clearly visible fiber pull-out. Such brushy fracture is typical of all specimens tested in tension-tension fatigue in this work. To gain greater insight into the effects of maximum stress and test environment on the composite microstructure and fracture surface topography, specimen fracture surfaces should be examined under an SEM. Such examination is strongly recommended for future work.

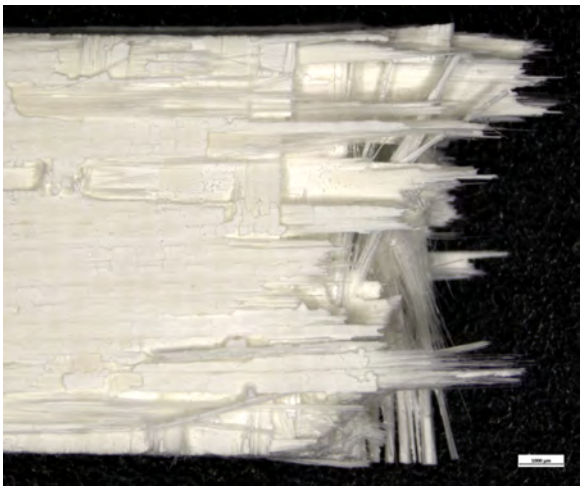

Figure 36. Optical micrograph of the fracture surface of N720/AM specimen tested in tension-tension fatigue at 1200°C in air. $\sigma_{max} = 100$ MPa, $N_f > 100000$.

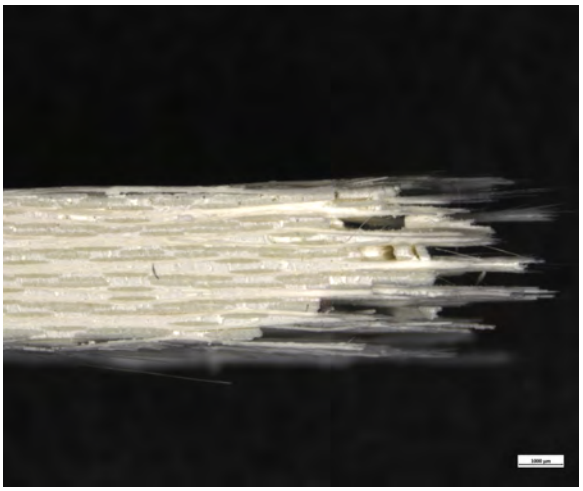

Figure 37. Optical micrograph of the fracture surface of N720/AM specimen tested in tension-tension fatigue at 1200°C in air. $\sigma_{max} = 100$ MPa, $N_f > 100000$.

4.2 Tension-Tension Fatigue Performance of Nextel^{TM} 720/A Specimens with Effusion Holes in Air and Steam at 1200°C

All tension-tension fatigue tests were conducted at 1.0 Hz with a sawtooth waveform. The ratio of the minimum stress to maximum stress was R = 0.05. Fatigue runout was set as 100,000 cycles. Such definition of fatigue runout permits direct comparison of the current study's results with those produced in previous AFIT studies on oxide/oxide CMC fatigue behavior [19][23][27].

Fatigue testing results of N720/A specimens with diamond-drilled (DD) holes performed in this study are summarized in Table 2. Results from a prior study of the fatigue behavior of unnotched, or un-drilled (UD), N720/A specimens [23] are included for comparison. Fatigue tests in this work were performed with the maximum stresses ranging from 100 to 150 MPa. It is noteworthy that all N720/A specimens with DD holes tested in fatigue in this work failed within the gage section of the extensometer. Harkins [6] reported a 1200°C ultimate tensile strength (UTS) for the N720/A DD specimens of 176 MPa. The tensile stress-strain curve for the N720/A with DD holes is shown in Figure 38. Note that the UTS for the unnotched N720/A specimens was previously reported as 193 MPa [23].

Results of the tension-tension fatigue tests on N720/A specimens with diamond-drilled (DD) holes are presented in Figure 39 as stress vs cycles to failure (S-N) curves. Results from prior work for the unnotched N720/A specimens [23] are included in Figure 39 for comparison. In air, the N720/A composite with an array of DD holes achieved fatigue runout in tests performed with the maximum stresses up to and including 120 MPa (68 %UTS at 1200°C). In steam, the fatigue runout of 100,000 cycles was achieved for the maximum stress of 100 MPa (57 %UTS at 1200°C). However, the DD specimen tested in steam with the maximum stress of 150 MPa failed after only 700 cycles. Additional tests would be required to determine the

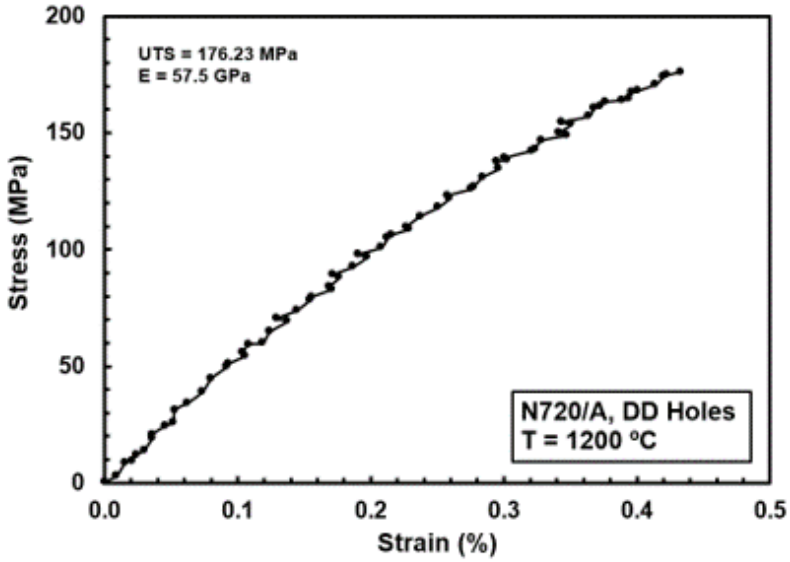

Figure 38. Tensile stress-strain curve at 1200°C for N720/A composite with an array of diamond-drilled holes [6]

fatigue limits in air and in steam. Unfortunately due to the short supply of test material, such additional tests could not be conducted as part of this effort.

Notably the fatigue limit for the unnotched N720/A specimens tested in air was a high 170 MPa (88 %UTS at 1200°C) [23]. Steam caused considerable degradation in the fatigue performance of the unnotched N720/A composite. The fatigue limit for the unnotched N720/A specimens tested in steam was only 125 MPa (65 %UTS at 1200°C).

When comparing results obtained for the DD specimens in this effort with the results obtained for the unnotched specimens in prior work, it is speculated that the presence of DD holes reduced the fatigue performance of the N720/A composite at 1200°C in both air and steam environments. It is likely that such decrease in the fatigue performance is not simply due to a lower UTS of the DD specimens. Of course additional DD specimens must be tested in air and in steam to confirm this conjecture.

Figure 40 shows the evolution of the stress-strain hysteresis response with cycles

Table 2. Summary of fatigue results for Diamond-Drilled and Un-Drilled N720/A composite at 1200°C, in laboratory air and steam environments

Test Environment	Maximum Stress (MPa)	Cycles to Failure (N)	Failure Strain (%)
DD, Fatigue at 1.0 Hz			
Laboratory air	106	179,620[a]	
Laboratory air	120	185,943[a]	2.54[a]
Steam	100	100,000[a]	0.95[a]
Steam	150	700	0.56
UD, Fatigue at 1.0 Hz[b]			
Laboratory air	100	120,199[a]	0.63[a]
Laboratory air	125	146.392[a]	1.14[a]
Laboratory air	150	167,473[a]	1.66[a]
Laboratory air	170	109,436[a]	2.25[a]
Steam	100	100,780[a]	0.71
Steam	125	166,326[a]	1.08
Steam	150	11,782	1.12
Steam	170	202	0.81

[a] Runout. Failure of the specimen did not occur when the test was terminated.
[b] Data from Ruggles-Wrenn et al, 2006[24].

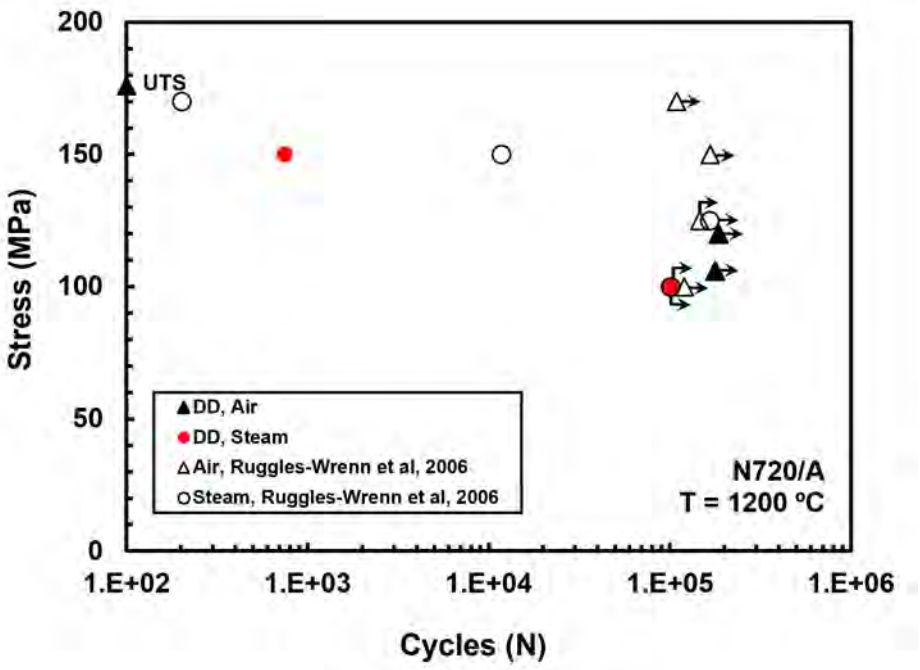

Figure 39. Fatigue S-N curves for N720/A specimens containing an array of DD holes and for N720/A unnotched specimens at 1200°C in air and in steam. Data for unnotched specimens from [23]. Arrows indicate that failure of the specimen did not occur when the test was terminated.

for the N720/A specimens with DD holes. Note that the most damage typically occurs on the first cycle. Then the hysteresis loops generally stabilize. Results in Figure 40 also reveal that ratchetting was observed for all tests. Similar behavior was reported for the unnotched N720/A specimens tested in tension-tension fatigue at 1200°C [23].

Figure 41 shows the strain accumulation with fatigue cycles count for the N720/A specimens with DD holes at 1200/degree C for air and steam environments. The largest strain was 2.54% accumulated by the specimen tested with maximum stress of 120 MPa in air, which exceeded fatigue runout by almost 86,000 cycles. The specimen with the shortest lifetime failed at 700 cycles under a maximum stress of 150 MPa in steam. Test data for this specimen revealed 0.56% strain accumulation at cycle 699 and 3.54% accumulation at cycle 700. This large increase in strain accumulation

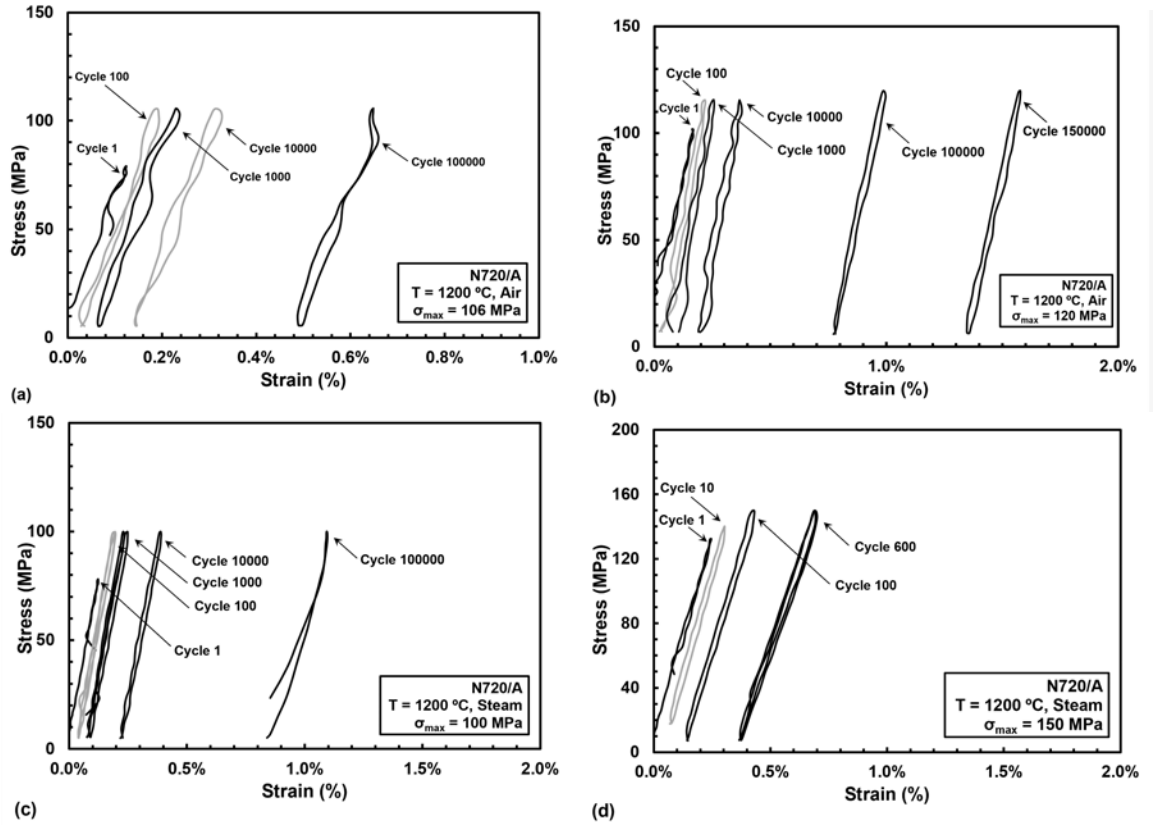

Figure 40. Typical evolution of stress-strain hysteresis response with fatigue cycles for N720/A specimens containing an array of DD holes at 1200°C: (a) air, σ_{max} = 106 MPa, (b) air, σ_{max} = 120 MPa, (c) steam, σ_{max} = 100 MPa, (d) steam, σ_{max} = 150 MPa.

was indicative of a rapidly developing damage that culminated in ultimate composite failure. All tests that achieved fatigue runout of 100,000 cycles represented in Figure 41 accumulated strains less than 2.54%. Nevertheless it is noted that ratcheting takes place in all tests conducted at 1200°C, regardless of whether the runout was achieved or not.

While three of the four specimens tested achieved a runout of 100,000 cycles, only one test was terminated as soon as the runout was achieved. The other two tests were allowed to fail in cyclic fatigue, albeit after having achieved cyclic lives considerably excess of 100,000 cycles. The test that was interrupted upon reaching 100,000 cycles without specimen failure was performed with the maximum stress of 100 MPa (57

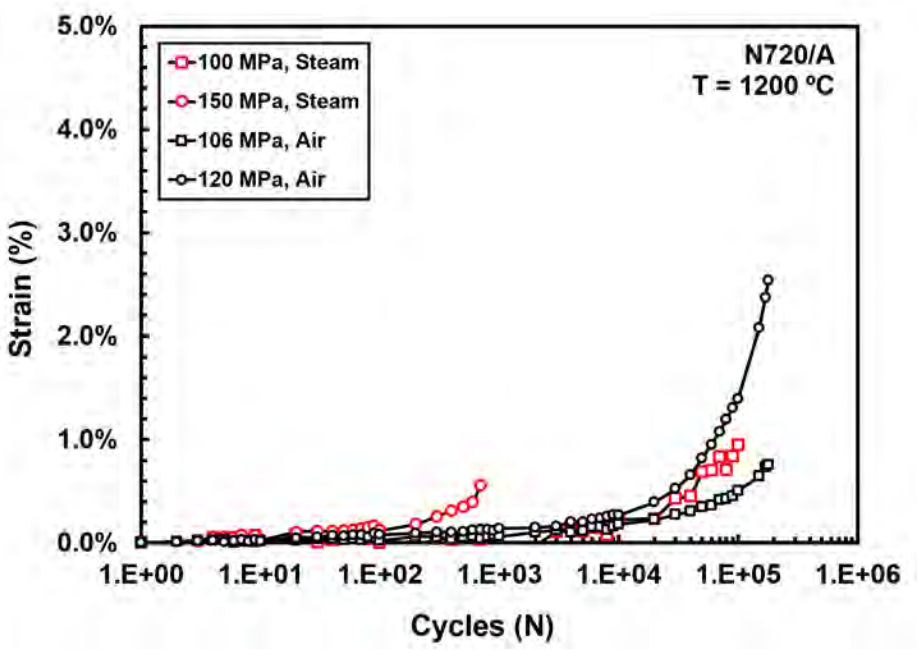

Figure 41. Strain accumulation with fatigue cycles for N720/A specimens containing an array of DD holes in air and steam at 1200°C.

%UTS) in steam. Following completion of 100,000 fatigue cycles, that specimen was tested in tension to failure at 1200°C to determine the retained strength. The specimen retained 75% of its tensile strength. It is noteworthy that the unnotched N720/A specimens tested in fatigue at 1200°C in air [23] retained 100% of their tensile strength, whereas the unnotched N720/A specimens tested in fatigue at 1200°C in steam retained over 85% of their tensile strength. Typically the loss of strength is associated with damage occurring to the reinforcing fibers. Clearly the N720/A specimen with DD holes lost a greater percentage of its tensile strength. In this case comminution of the matrix in the vicinity of the holes caused by diamond-drilling may be contributing to the loss of the composite's strength.

Due to limited strain accumulation and high cyclic lifetimes, it can be deduced that for the tests at 106 and 120 MPa in air and 100 MPa in steam, the specimens' modulus of elasticity was minimally decreased prior to reaching 100,000 cycles.

The diamond-drilled N720/A specimen tested in tension-tension fatigue in air

with the maximum stress of 150 MPa and failed after 700 cycles was examined under an optical microscope, seen in Figures 42 and 43. Optical micrographs reveal fibrous fracture with clear fiber pull-out, similar to that of the N720/AM composite. The high maximum stress level had a catastrophic impact on fibrous material. It is apparent that the larger maximum stress value damaged the load-bearing fibers more than the fatigue test with a maximum stress of 120 MPa in air, seen in Figure 44. SEM examination is strongly recommended for future work.

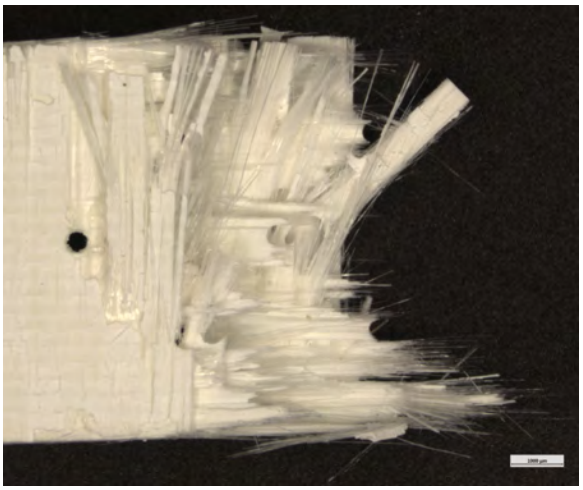

Figure 42. Optical micrograph of the fracture surface of N720/AM specimen tested in tension-tension fatigue at 1200°C in steam. σ_{max} = 150 MPa, N_f = 700.

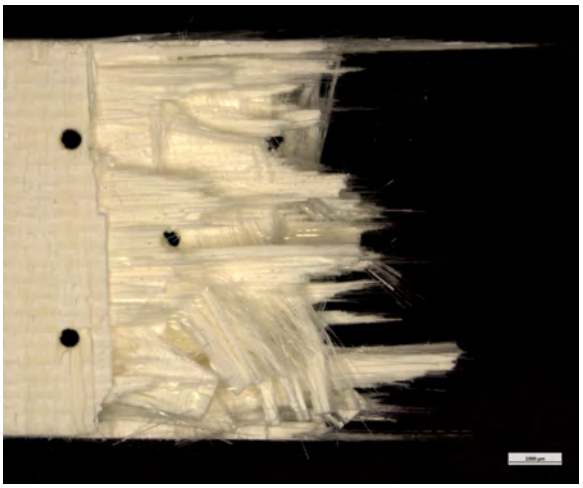

Figure 43. Optical micrograph of the fracture surface of N720/AM specimen tested in tension-tension fatigue at 1200°C in steam. σ_{max} = 150 MPa, N_f = 700.

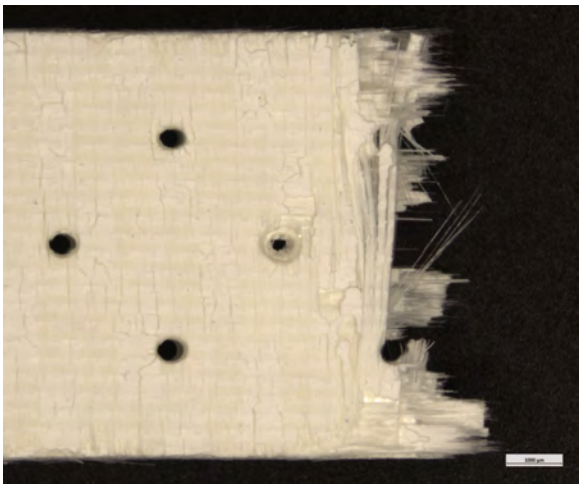

Figure 44. Optical micrograph of the fracture surface of N720/AM specimen tested in tension-tension fatigue at 1200°C in air. σ_{max} = 120 MPa, N_f = 185943.

4.3 Tension to failure of single-lap-joint brazed N720/A specimens

Single-lap-joint brazed N720/A specimens were tested in tension to failure to determine the tensile strength of the brazed joint and to assess the feasibility of brazing as a technique to join CMCs. All tension to failure tests of the brazed specimens were conducted in displacement control at a rate of 0.02 mm/s in laboratory air. To assess the effects of temperature on the brazed joint's tensile strength, tension tests were performed at 23°, 550° and 650°C.

Brazing experts at Morgan Advanced Materials expected the brazed joint to have good load-bearing capacity at temperatures up to and including 650°C. However, tension tests revealed that the tensile strength of the brazed joint was less than 2 MPa at 23°, 550° and 650°C. Such exceptionally low tensile strength values demonstrate that brazing is not an acceptable technique to join CMCs.

The tested Nextel 720/A brazed specimens were examined to determine whether manufacturing defects were the cause of early failure. Optical microscopy revealed poor bonding between the braze alloy and CMC material. Most, if not all, of the braze alloy remained attached to one side of the single-lap-joint, leaving the other side

virtually clean (see Figure 45 and Figure 46). Based on these results, it is determined that this particular brazing technique is not acceptable for joining CMCs.

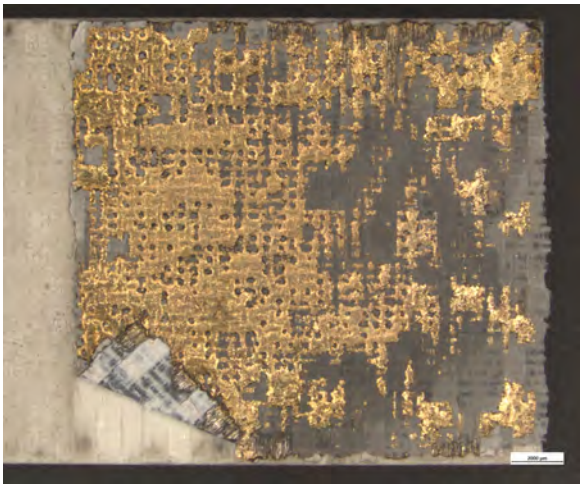

Figure 45. Top section of brazed joint

Figure 46. Bottom section of brazed joint

V. Conclusions and Recommendations

5.1 Conclusions

The tension-tension fatigue behavior of N720/AM composite was examined at 1200°C in a laboratory air environment. Fatigue tests were performed at 1.0 Hz. Fatigue runout of 100,000 cycles was achieved for maximum stress levels ranging from 100 to 140 MPa. The specimen loaded with a maximum fatigue stress of 140 MPa and which achieved cyclic runout, was subsequently tested in tension to failure at 1200°C to determine the retained tensile strength. This specimen retained 100% of its tensile strength indicating that no damage occurred to the fibers during prior fatigue.

The tension-tension fatigue behavior of N720/A composite material with diamond-drilled effusion holes was examined at 1200°C. Fatigue tests were conducted with a loading frequency of 1.0 Hz in laboratory air and steam environments. The presence of the DD holes appears to degrade fatigue performance of the N720/A composite. At 1200°C in air, fatigue runout of 100,000 cycles was achieved under maximum stresses of 106 and 120 MPa (68 %UTS). Notably, the unnotched N720/A composite produced a much higher fatigue limit of 170 MPa (88 %UTS) at 1200°C in air. The steam environment had a detrimental effect on the fatigue performance of N720/A specimens with DD holes. In steam, fatigue runout was achieved for the maximum stress of 100 MPa (57 %UTS). However, the specimen tested in steam with the maximum stress of 150 MPa survived only 700 cycles. Pulverization of the matrix material in the vicinity of DD holes is behind the degradation of N720/A's tension-tension fatigue performance. However, additional testing is needed to determine the fatigue limits in air and in steam. Unfortunately due to the short supply of test material, such additional tests could not be conducted as a part of this effort.

Single-lap-joint brazed N720/A specimens were tested in tension to failure at 23°, 550° and 650°C in laboratory air to measure the tensile strength of the brazed CMC joint. The average tensile strength of the brazed joint was approximately 2.0 MPa regardless of test temperature. Such exceptionally low tensile strength of the brazed joint was attributed to poor bonding between the braze alloy and the parent CMC material. This effort concludes that the specific brazing technique used to prepare the test specimens for this work is not a feasible technique for joining CMCs. Other joining methods should be explored.

5.2 Recommendations

If brazing is a desired technique for joining CMCs for aerospace applications, brazing alloys and procedures that allow braze permeation and adequate infiltration into parent material, must be found. Brazing processes that do not create a strong bond between braze alloy and parent material will not survive the harsh environments of aerospace applications.

With regards to tension-tension fatigue testing of CMCs, this effort was limited by the number of available test specimens. More specimens are needed to fully characterize the fatigue performance of N720/A with DD effusion holes and that of the N720/AM composite. In addition, the specimens designed for this effort were based on a previous laboratory setup utilizing a smaller furnace. This effort would have greatly benefited from specimens that were longer in length to account for larger dimensions of the new furnace. Additionally, failed specimens should be examined under a scanning electron microscope to further characterize fracture surfaces and damage and failure mechanisms.

Appendix A. Composite Micrographs

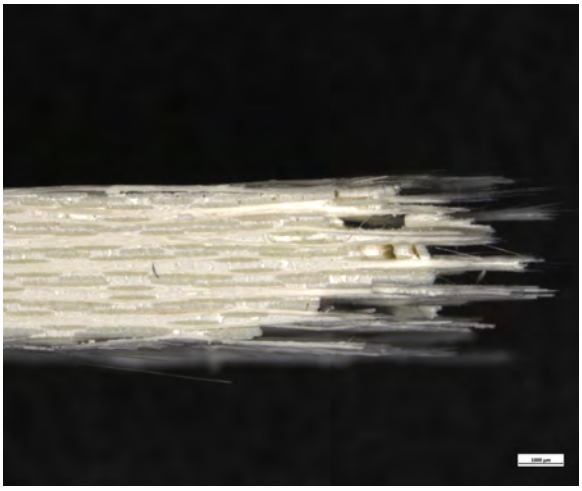

Figure 47. Optical micrograph of a N720/AM specimen fracture surface tested in tension-tension fatigue at 1200°C in air. σ_{max} = 100 MPa, N_f = 107,829

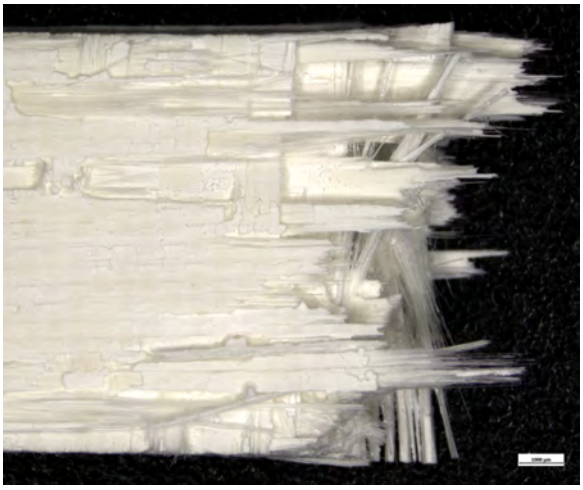

Figure 48. Optical micrograph of a N720/AM specimen fracture surface tested in tension-tension fatigue at 1200°C in air. σ_{max} = 100 MPa, N_f = 107,829

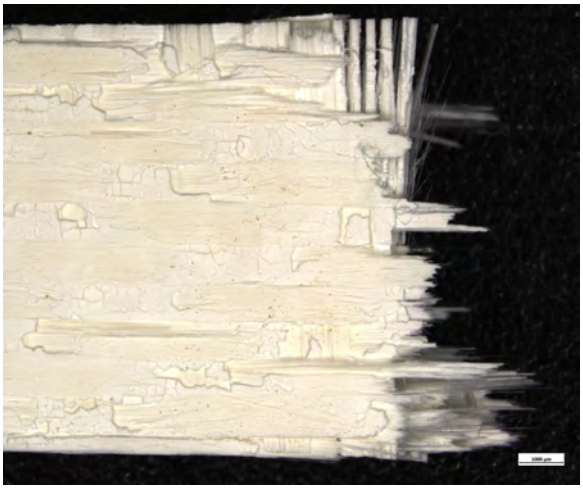

Figure 49. Optical micrograph of a N720/AM specimen fracture surface tested in tension-tension fatigue at 1200°C in air. σ_{max} = 100 MPa, N_f = 107,829

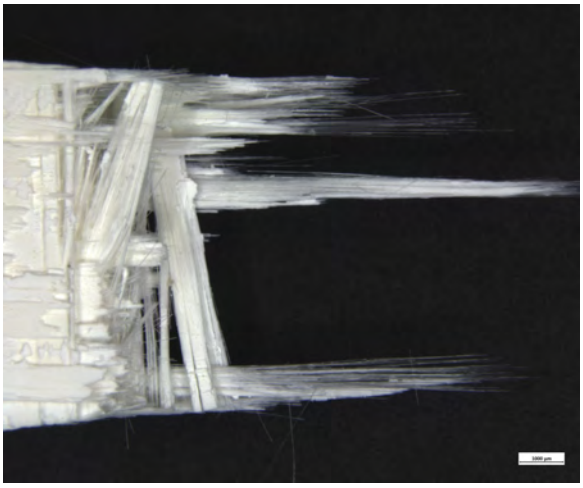

Figure 50. Optical micrograph of a N720/AM specimen fracture surface tested in tension-tension fatigue at 1200°C in air. σ_{max} = 100 MPa, N_f = 107,829

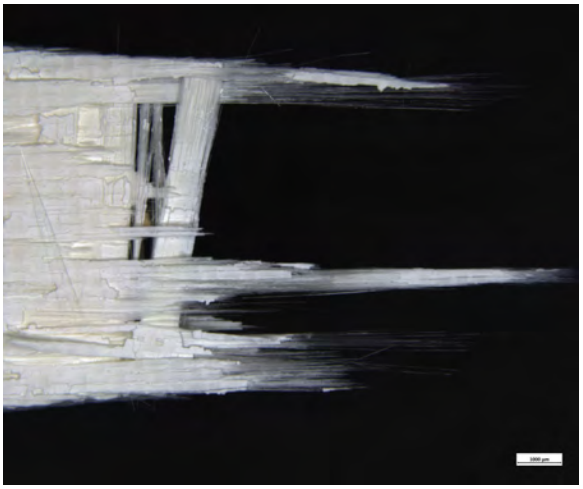

Figure 51. Optical micrograph of a N720/AM specimen fracture surface tested in tension-tension fatigue at 1200°C in air. σ_{max} = 100 MPa, N_f = 107,829

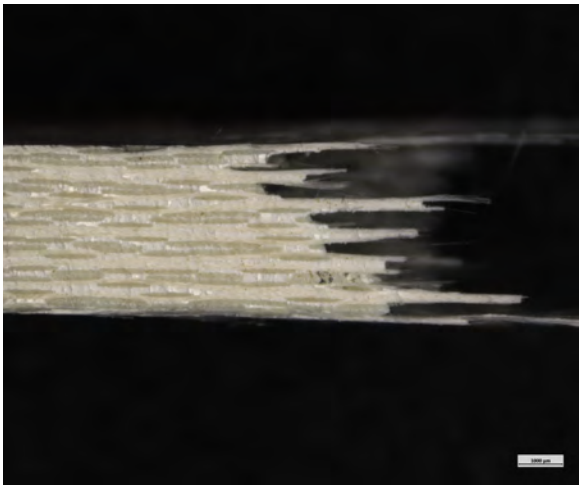

Figure 52. Optical micrograph of a N720/AM specimen fracture surface tested in tension-tension fatigue at 1200°C in air. σ_{max} = 120 MPa, N_f >100,000

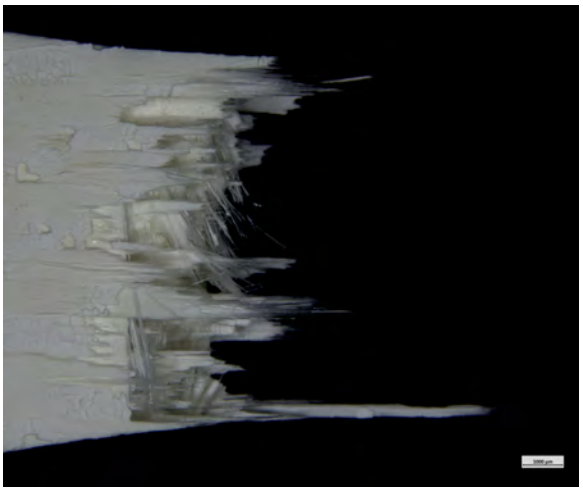

Figure 53. Optical micrograph of a N720/AM specimen fracture surface tested in tension-tension fatigue at 1200°C in air. σ_{max} = 120 MPa, N_f >100,000

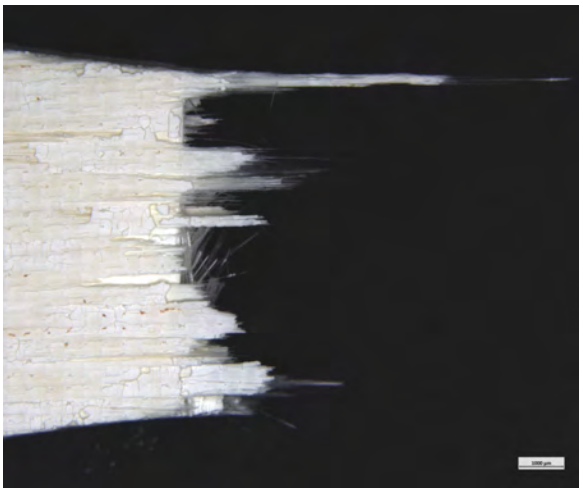

Figure 54. Optical micrograph of a N720/AM specimen fracture surface tested in tension-tension fatigue at 1200°C in air. σ_{max} = 120 MPa, N_f >100,000

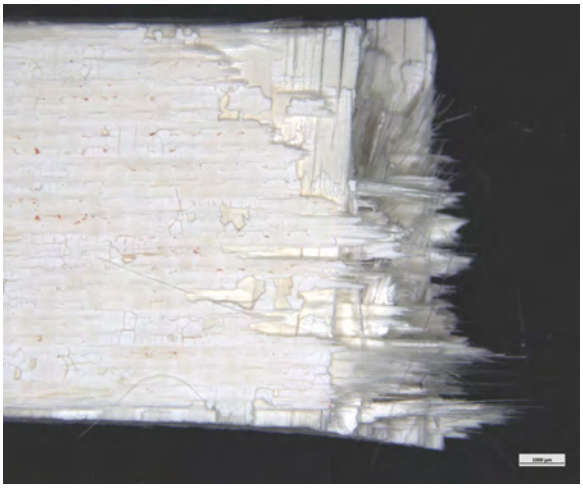

Figure 55. Optical micrograph of a N720/AM specimen fracture surface tested in tension-tension fatigue at 1200°C in air. σ_{max} = 120 MPa, N_f >100,000

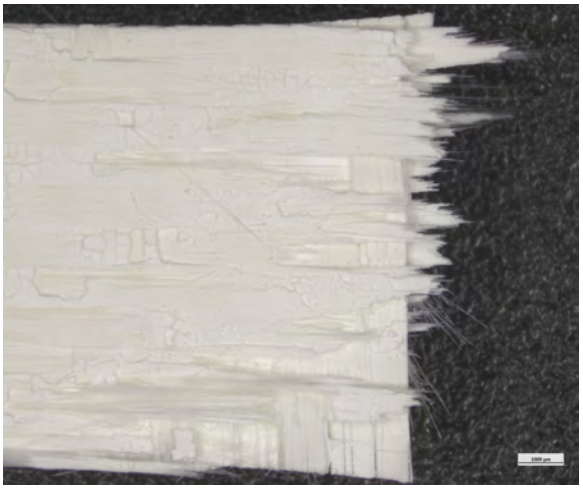

Figure 56. Optical micrograph of a N720/AM specimen fracture surface tested in tension-tension fatigue at 1200°C in air. σ_{max} = 120 MPa, N_f >100,000

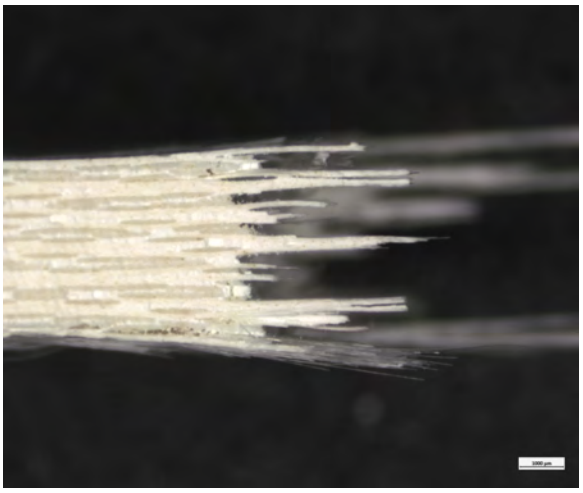

Figure 57. Optical micrograph of a N720/AM specimen fracture surface tested in tension-tension fatigue at 1200°C in air. σ_{max} = 130 MPa, N_f >100,000

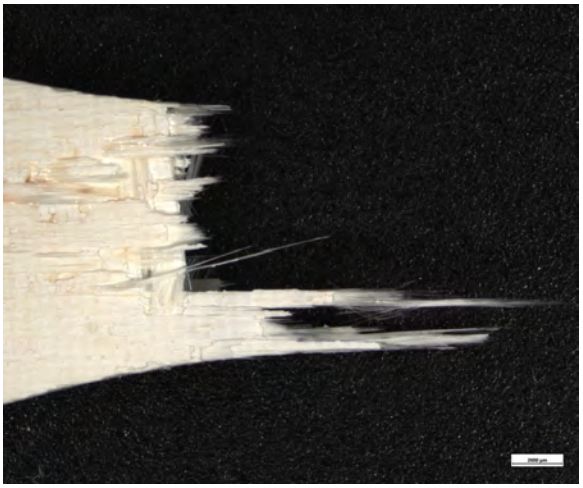

Figure 58. Optical micrograph of a N720/AM specimen fracture surface tested in tension-tension fatigue at 1200°C in air. σ_{max} = 130 MPa, N_f >100,000

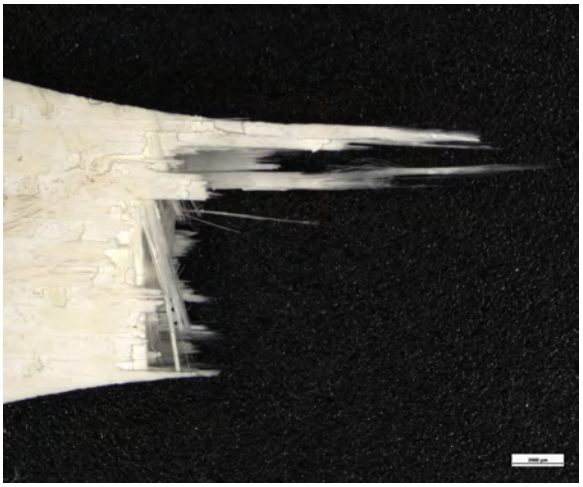

Figure 59. Optical micrograph of a N720/AM specimen fracture surface tested in tension-tension fatigue at 1200°C in air. σ_{max} = 130 MPa, N_f >100,000

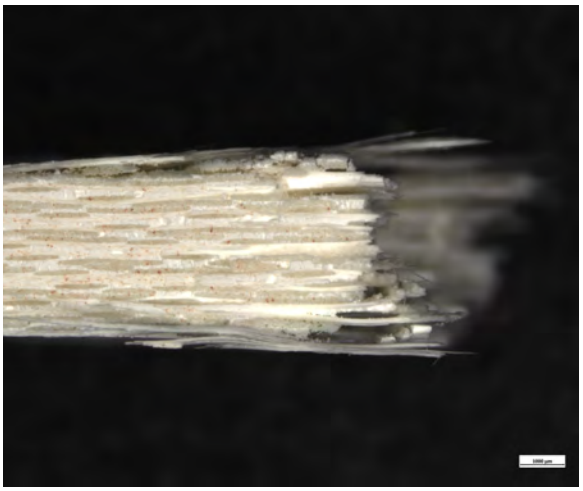

Figure 60. Optical micrograph of a N720/AM specimen fracture surface tested in tension-tension fatigue at 1200°C in air. σ_{max} = 130 MPa, N_f >100,000

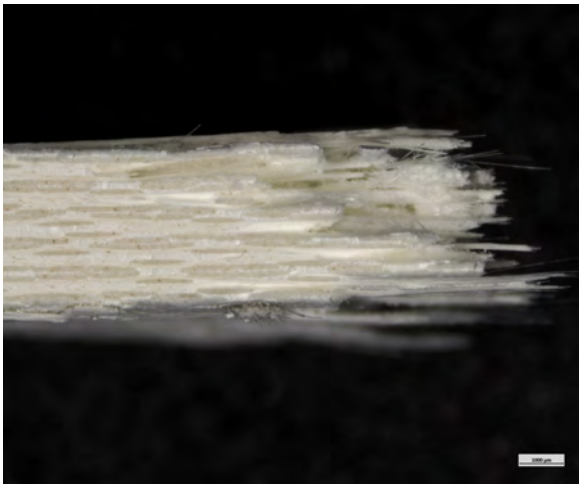

Figure 61. Optical micrograph of a N720/AM specimen fracture surface tested in tension-tension fatigue at 1200°C in air. σ_{max} = 130 MPa, N_f >100,000

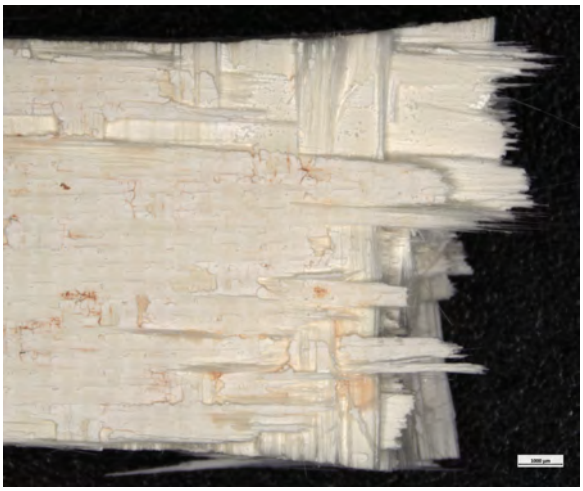

Figure 62. Optical micrograph of a N720/AM specimen fracture surface tested in tension-tension fatigue at 1200°C in air. σ_{max} = 130 MPa, N_f >100,000

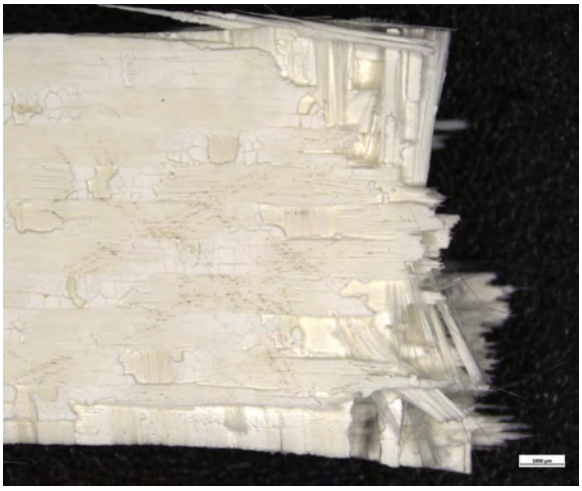

Figure 63. Optical micrograph of a N720/AM specimen fracture surface tested in tension-tension fatigue at 1200°C in air. σ_{max} = 130 MPa, N_f >100,000

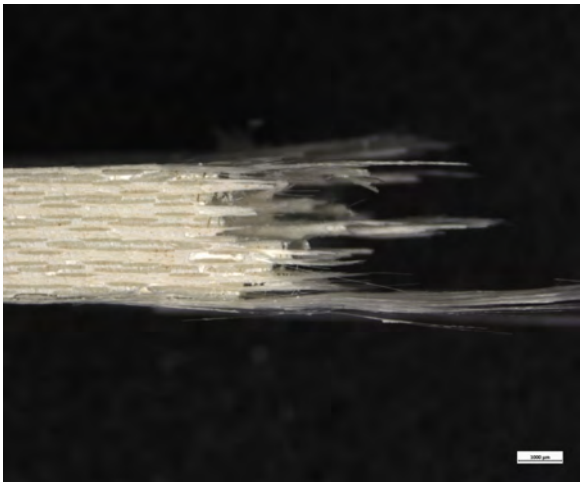

Figure 64. Optical micrograph of a N720/AM specimen fracture surface tested in tension-tension fatigue at 1200°C in air. σ_{max} = 140 MPa, N_f >100,000

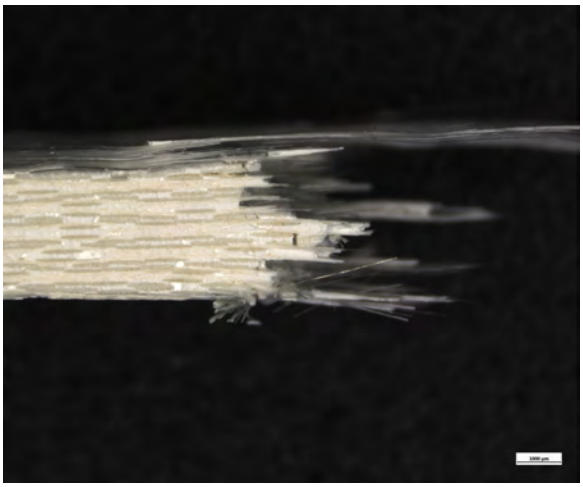

Figure 65. Optical micrograph of a N720/AM specimen fracture surface tested in tension-tension fatigue at 1200°C in air. σ_{max} = 140 MPa, N_f >100,000

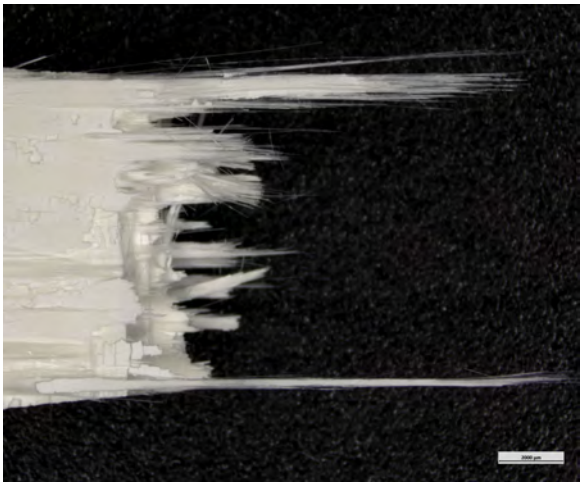

Figure 66. Optical micrograph of a N720/AM specimen fracture surface tested in tension-tension fatigue at 1200°C in air. σ_{max} = 140 MPa, N_f >100,000

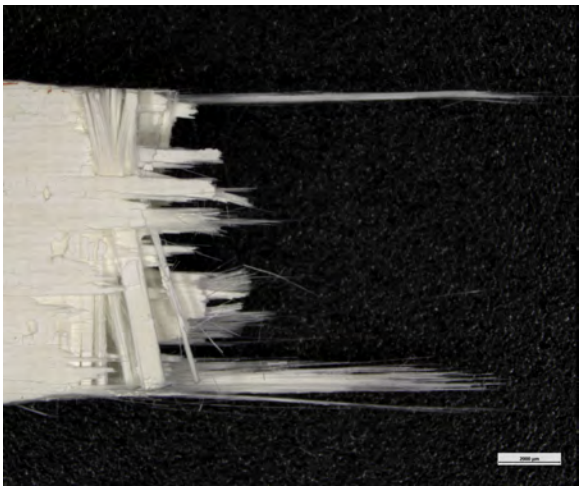

Figure 67. Optical micrograph of a N720/AM specimen fracture surface tested in tension-tension fatigue at 1200°C in air. σ_{max} = 140 MPa, N_f >100,000

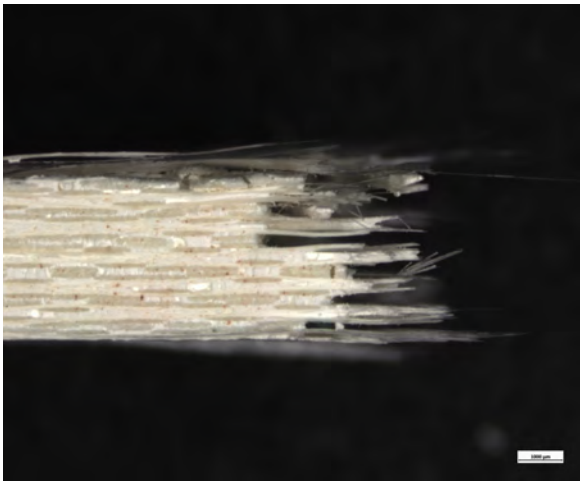

Figure 68. Optical micrograph of a N720/AM specimen fracture surface tested in tension-tension fatigue at 1200°C in air. σ_{max} = 140 MPa, N_f >100,000

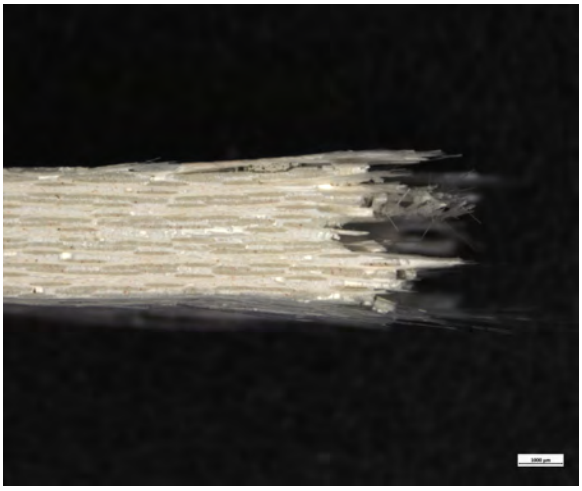

Figure 69. Optical micrograph of a N720/AM specimen fracture surface tested in tension-tension fatigue at 1200°C in air. σ_{max} = 140 MPa, N_f >100,000

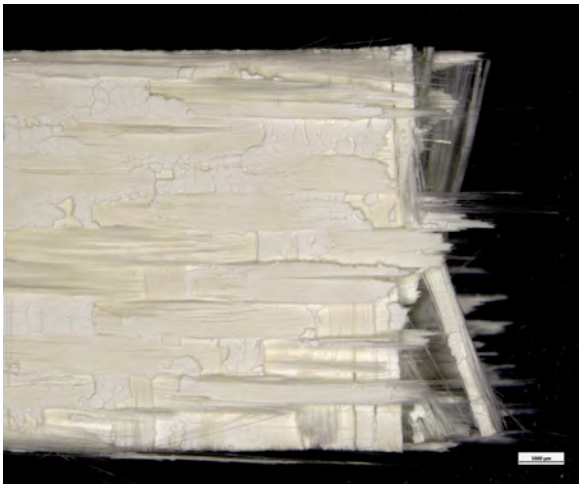

Figure 70. Optical micrograph of a N720/AM specimen fracture surface tested in tension-tension fatigue at 1200°C in air. σ_{max} = 140 MPa, N_f >100,000

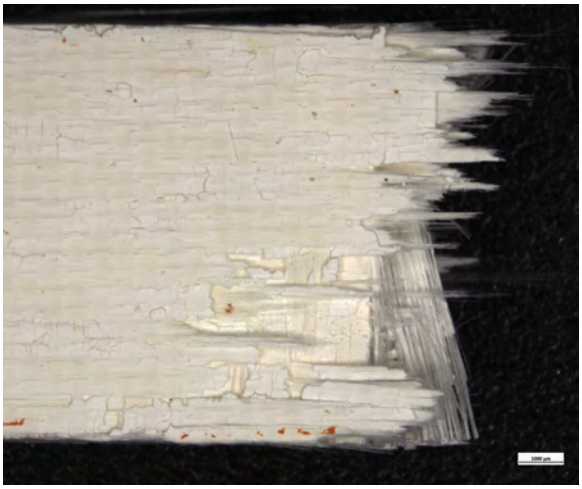

Figure 71. Optical micrograph of a N720/AM specimen fracture surface tested in tension-tension fatigue at 1200°C in air. σ_{max} = 140 MPa, N_f >100,000

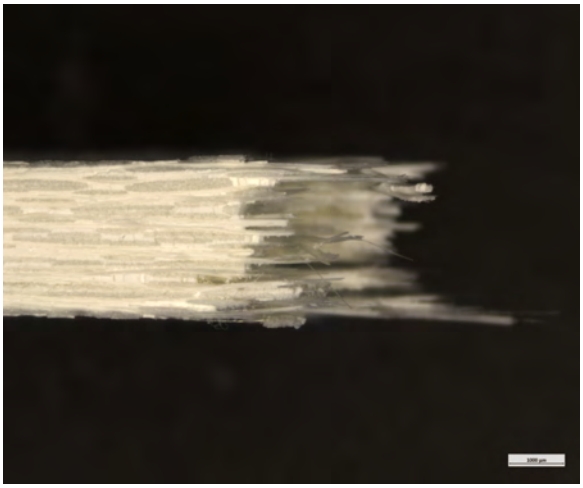

Figure 72. Optical micrograph of a N720/A specimen fracture surface tested in tension-tension fatigue at 1200°C in air. σ_{max} = 120 MPa, N_f = 185,943

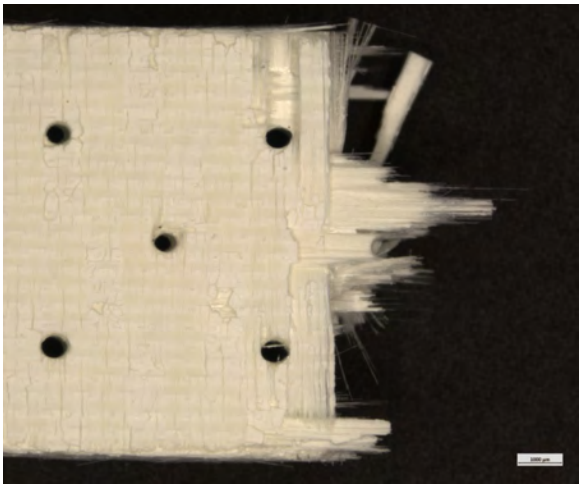

Figure 73. Optical micrograph of a N720/A specimen fracture surface tested in tension-tension fatigue at 1200°C in air. σ_{max} = 120 MPa, N_f = 185,943

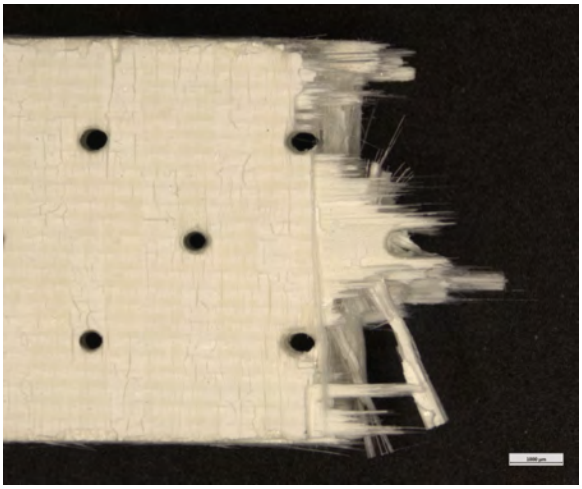

Figure 74. Optical micrograph of a N720/A specimen fracture surface tested in tension-tension fatigue at 1200°C in air. σ_{max} = 120 MPa, N_f = 185,943

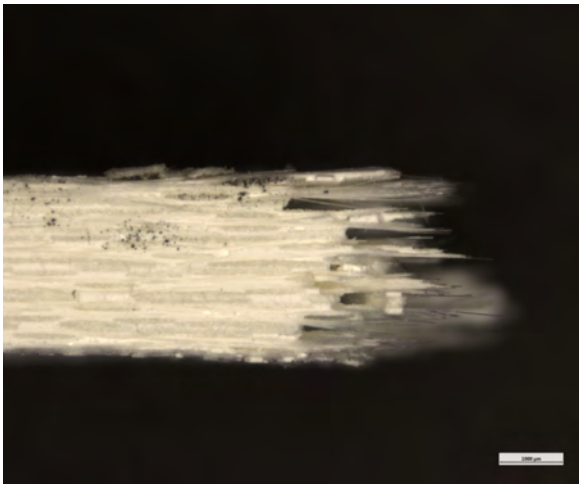

Figure 75. Optical micrograph of a N720/A specimen fracture surface tested in tension-tension fatigue at 1200°C in air. σ_{max} = 120 MPa, N_f = 185,943

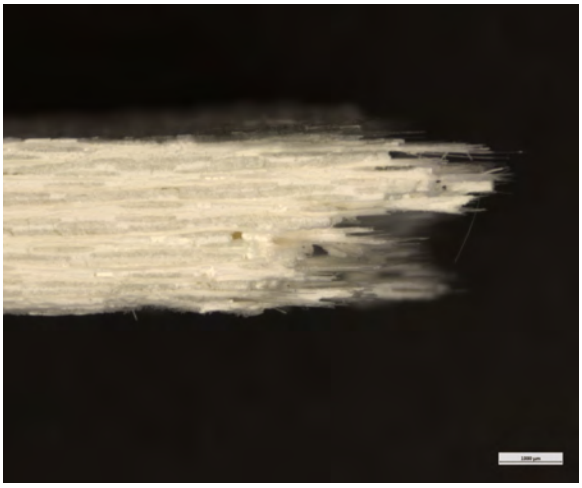

Figure 76. Optical micrograph of a N720/A specimen fracture surface tested in tension-tension fatigue at 1200°C in air. σ_{max} = 120 MPa, N_f = 185,943

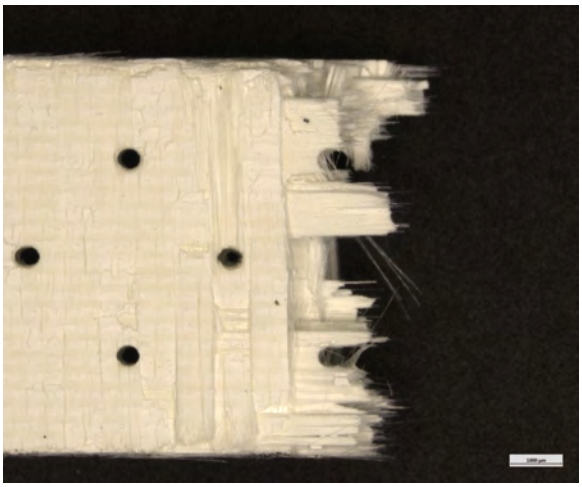

Figure 77. Optical micrograph of a N720/A specimen fracture surface tested in tension-tension fatigue at 1200°C in air. σ_{max} = 120 MPa, N_f = 185,943

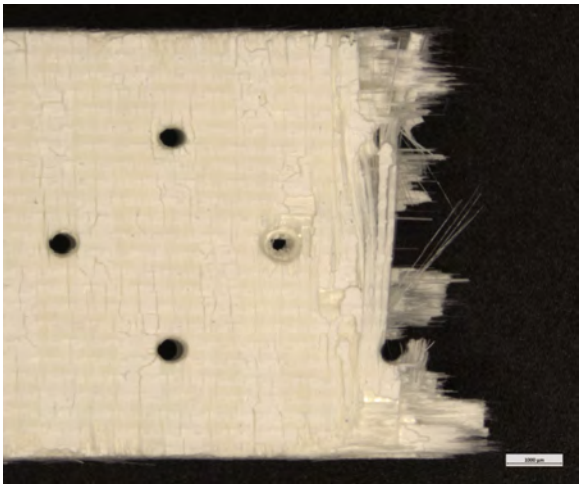

Figure 78. Optical micrograph of a N720/A specimen fracture surface tested in tension-tension fatigue at 1200°C in air. σ_{max} = 120 MPa, N_f = 185,943

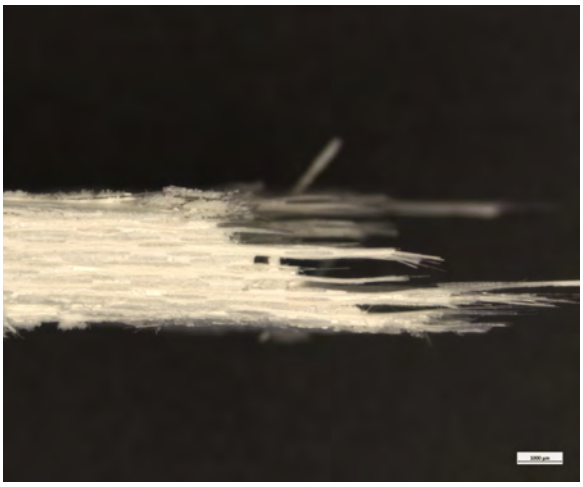

Figure 79. Optical micrograph of a N720/A specimen fracture surface tested in tension-tension fatigue at 1200°C in steam. σ_{max} = 100 MPa, N_f >100,000

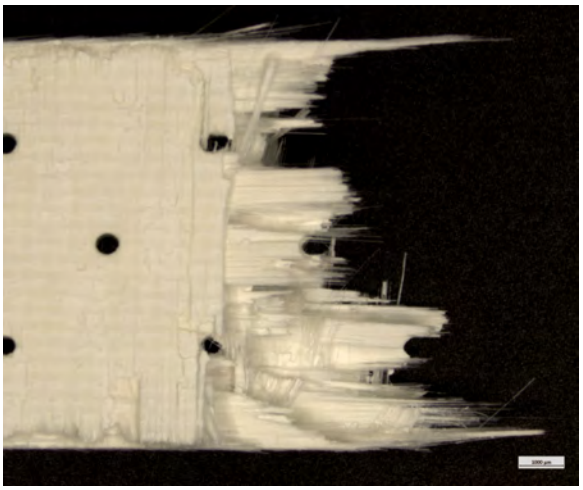

Figure 80. Optical micrograph of a N720/A specimen fracture surface tested in tension-tension fatigue at 1200°C in steam. σ_{max} = 100 MPa, N_f >100,000

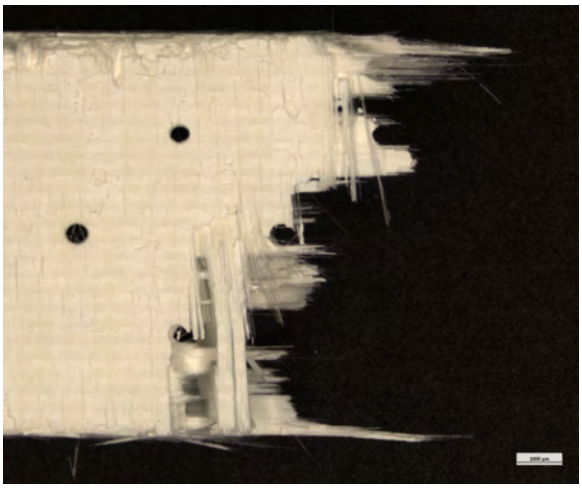

Figure 81. Optical micrograph of a N720/A specimen fracture surface tested in tension-tension fatigue at 1200°C in steam. σ_{max} = 100 MPa, N_f >100,000

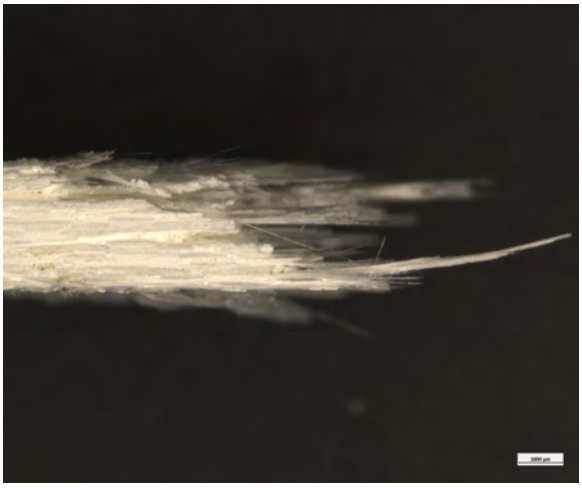

Figure 82. Optical micrograph of a N720/A specimen fracture surface tested in tension-tension fatigue at 1200°C in steam. σ_{max} = 100 MPa, N_f >100,000

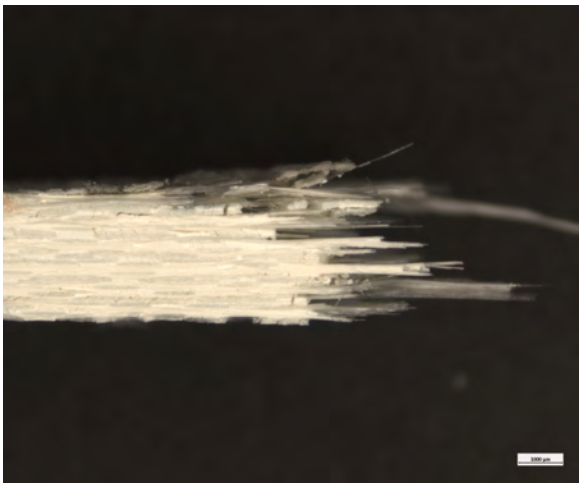

Figure 83. Optical micrograph of a N720/A specimen fracture surface tested in tension-tension fatigue at 1200°C in steam. σ_{max} = 100 MPa, N_f >100,000

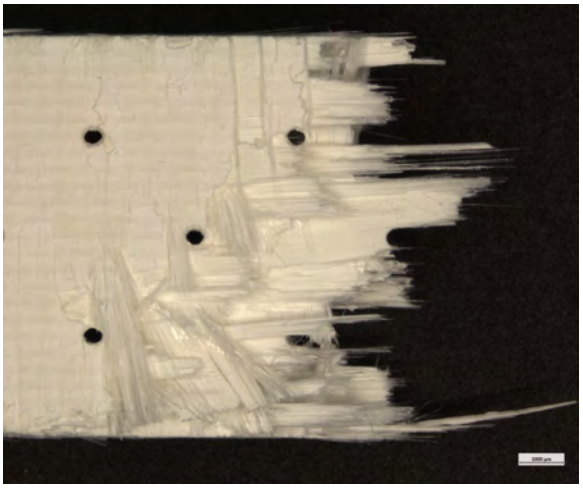

Figure 84. Optical micrograph of a N720/A specimen fracture surface tested in tension-tension fatigue at 1200°C in steam. σ_{max} = 100 MPa, N_f >100,000

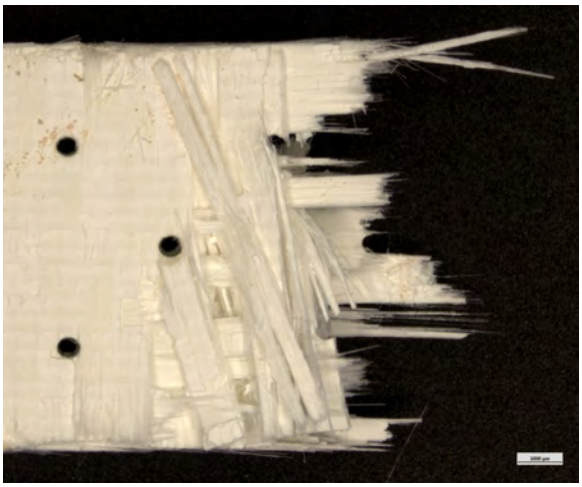

Figure 85. Optical micrograph of a N720/A specimen fracture surface tested in tension-tension fatigue at 1200°C in steam. σ_{max} = 100 MPa, N_f >100,000

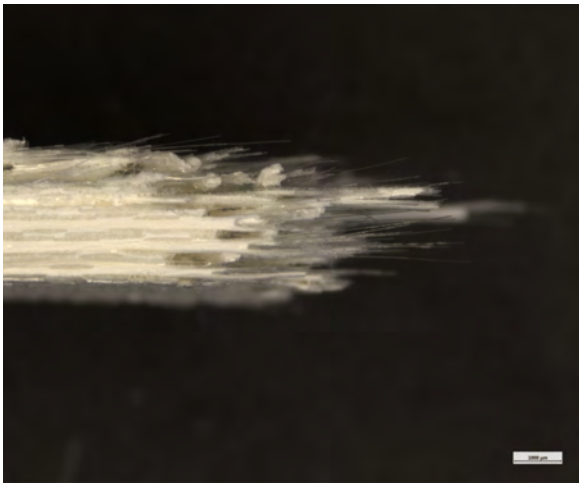

Figure 86. Optical micrograph of a N720/A specimen fracture surface tested in tension-tension fatigue at 1200°C in steam. σ_{max} = 150 MPa, N_f = 700

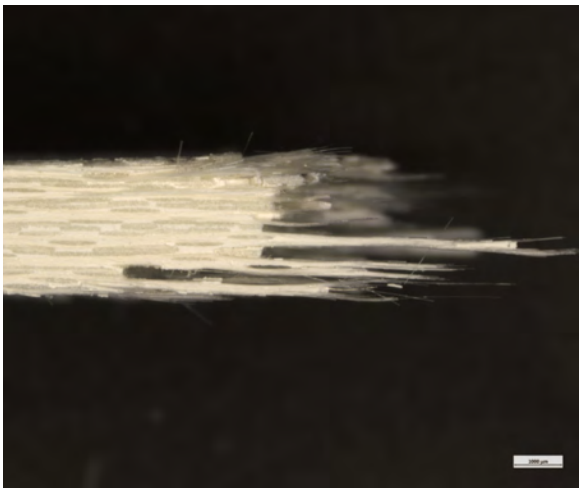

Figure 87. Optical micrograph of a N720/A specimen fracture surface tested in tension-tension fatigue at 1200°C in steam. σ_{max} = 150 MPa, N_f = 700

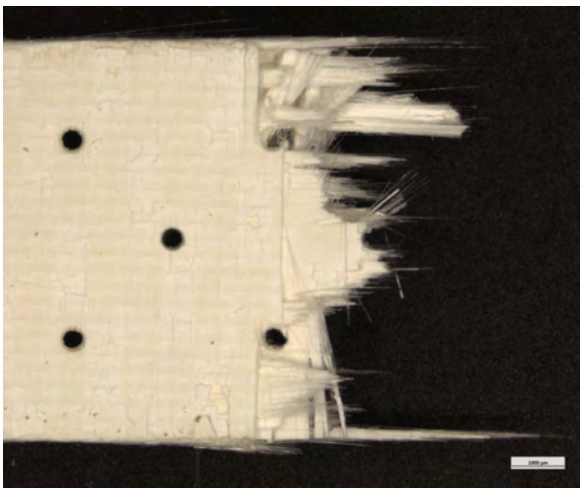

Figure 88. Optical micrograph of a N720/A specimen fracture surface tested in tension-tension fatigue at 1200°C in steam. σ_{max} = 150 MPa, N_f = 700

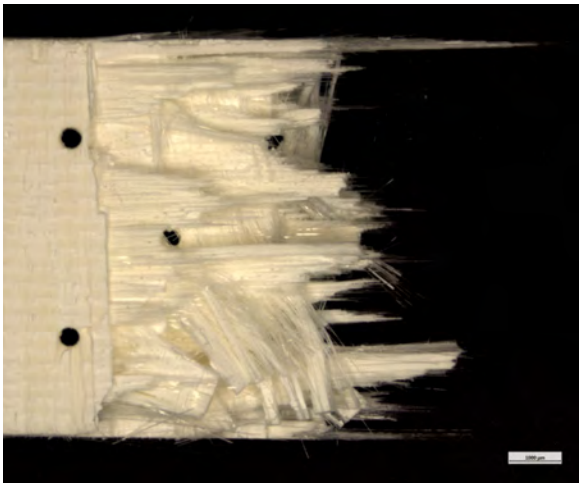

Figure 89. Optical micrograph of a N720/A specimen fracture surface tested in tension-tension fatigue at 1200°C in steam. σ_{max} = 150 MPa, N_f = 700

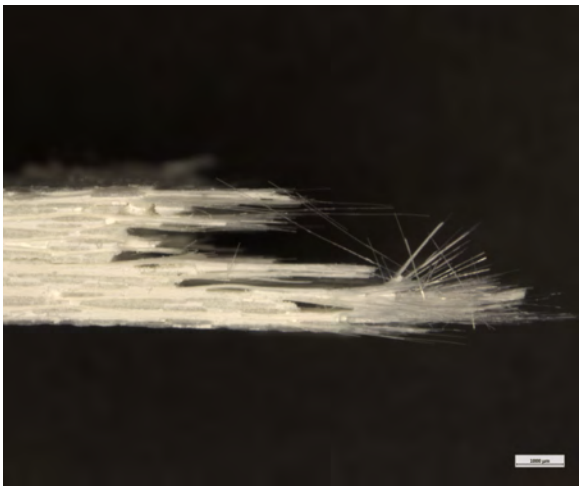

Figure 90. Optical micrograph of a N720/A specimen fracture surface tested in tension-tension fatigue at 1200°C in steam. σ_{max} = 150 MPa, N_f = 700

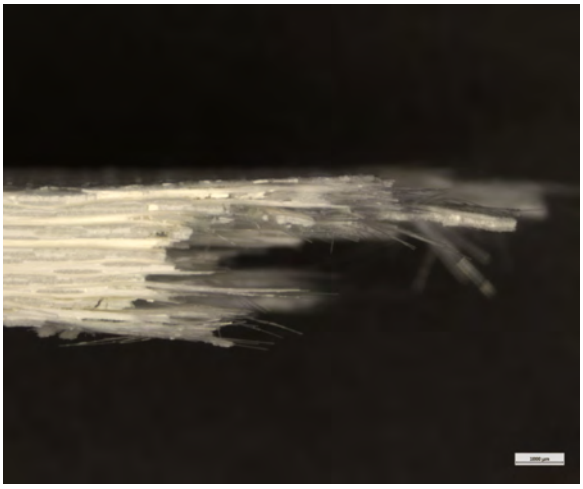

Figure 91. Optical micrograph of a N720/A specimen fracture surface tested in tension-tension fatigue at 1200°C in steam. $\sigma_{max} = 150$ MPa, $N_f = 700$

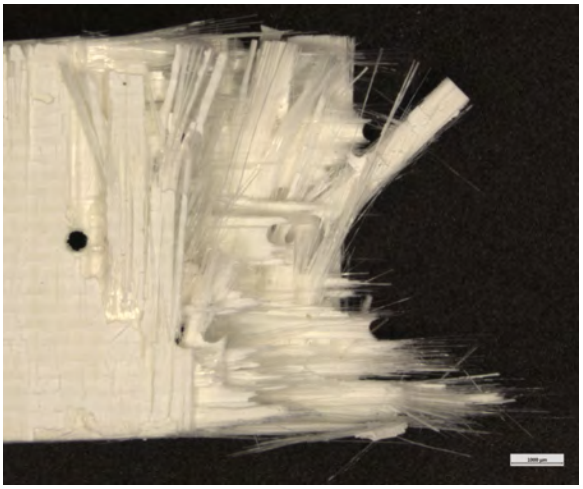

Figure 92. Optical micrograph of a N720/A specimen fracture surface tested in tension-tension fatigue at 1200°C in steam. $\sigma_{max} = 150$ MPa, $N_f = 700$

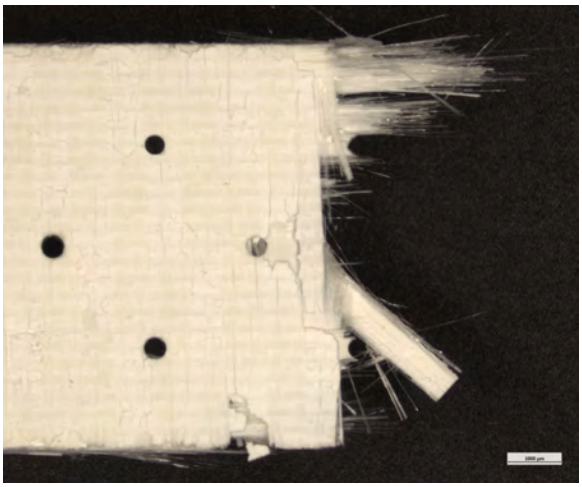

Figure 93. Optical micrograph of a N720/A specimen fracture surface tested in tension-tension fatigue at 1200°C in steam. σ_{max} = 150 MPa, N_f = 700

Bibliography

1. 3M Advanced Materials Division [n.d.], '3m^{TM} nextel^{TM} ceramic fibers and textiles - technical reference guide'.
   URL: *https://multimedia.3m.com/mws/media/1327055O/3m-nextel-technical-reference-guide.pdf*

2. Akram, M., Ferraris, M., Casalegno, V., Salvo, M., Puchas, G., Knohl, S. and Krenkel, W. [n.d.], 'Joining and testing of alumina fibre reinforced yag-zro$_2$ matrix composites'.

3. Asthana, R. and Singh, M. [2013], 'Active metal brazing of advanced ceramic composites to metallic systems', *Advances in Brazing - Science, Technology and Applications; A volume in Woodhead Publishing Series in Welding and Other Joining Technologies* pp. 323–360.

4. Chawla, K. [1993], *Ceramic Matrix Composites*, 1 edn, Springer. Affiliation: Department of Material and Metallurgical Engineering, New Mexico Institute of Mining and Technology, Socorro, USA.

5. Genelin, C. [2008], Effects of environment on creep behavior of nextel 720/alumina-mullite ceramic composite at 1200°c, Master's thesis, Air Force Institute of Technology, 2950 Hobson Way, Wright-Patterson AFB, OH 45433, United States. An optional note.

6. Harkins, M. L. [2019], Creep of nextel 720/alumina ceramic matrix composite with diamond-drilled effusion holes at 1200°c in air and in steam, Master's thesis, Air Force Institute of Technology, Air University, 2950 Hobson Way, Wright-Patterson AFB, OH 45433, United States. An optional note.

7. Isaac M. Daniel, O. I. [2006], *Engineering Mechanics of Composite Materials*, Vol. 4 of *10*, 2 edn, Oxford University Press, Inc., 198 Madison Avenue, New York, New York 10016.

8. Jurf, R. and Butner, S. [1999], 'Advances in oxide-oxide cmc', *Proceedings of the 44^{TM} ASME 1999 International Gas Turbine and Aeroengine Congress and Exhibition* **Volume 4: Manufacturing Materials and Metallurgy; Ceramics; Structures and Dynamics; Controls, Diagnostics and Instrumentation**.

9. Kutsal, T. and Ruggles-Wrenn, M. [2010], 'Effects of steam environment on creep behavior of nextel^{TM} 720/alumina-mullite ceramic composite at elevated temperature', *Composites Part A: Applied Science and Manufacturing* **41**, 1807–1816.

10. Materials, M. A. [n.d.], 'Morgan advanced materials, wesgo - data sheet'.
    URL: *https://www.morganbrazealloys.com/media/6941/wesgo$_c$usil − aba$_t$echnical − data − sheet − 2018.pdf*

11. Michael C. Halbig, Mrityunjay Singh [n.d.], 'Joining and integration of silicon carbide-based materials for high temperature applications'.
URL: *https://ntrs.nasa.gov/search.jsp?R=20160010279*

12. Micro-Measurements, Vishay Precision Group, I. [n.d.], 'M-bond 200, strain gage adhesive'.
URL: *http://www.vishaypg.com/docs/11010/bond200.pdf*

13. Minor, S. N. [2018], Creep of nextel 720/a ceramic matrix composite with laser driller effusion holes at 1200°c in air and in steam, Master's thesis, Air Force Institute of Technology, Air University, 2950 Hobson Way, Wright-Patterson AFB, OH 45433, United States. An optional note.

14. Naidich, Y., Zhuravlev, V., Gab, I., Kostyuk, B., Krasovskyy, V., Adamovskyy, A. and Taranets, N. [2008], 'Liquid metal wettability and advanced ceramic brazing', *Journal of the European Ceramic Society* **28**, 717–728.

15. Ozer, M. [2010], 'Creep behavior of nextel^{TM} 720/alumina-mullite ceramic composite with +/-45°fiber orientation at 1200°c', *Materials Science and Engineering: A* **527**, 5326–5334.

16. Ruggles-Wrenn, M. B. [2018], 'Mechanical behavior of oxide-oxide fiber-reinforced cmcs at elevated temperature: Environmental effects', *Comprehensive Composite Materials II* **5**, 174–236.

17. Ruggles-Wrenn, M. B., Minor, S. N., Przybyla, C. P. and Jones, E. L. [2019], 'Creep of a nextel^{TM} 720/alumina ceramic composite containing an arrary of small holes at 1200°c in air and in steam', *International Journal of Applied Ceramic Technology* **16**, 3–13.

18. Ruggles-Wrenn, M. and Genelin, C. [2009], 'Creep of nextel^{TM} 720/alumina-mullite ceramic composite at 1200°c in air, argon, and steam', *Composites Science and Technology* **69**, 663–669.

19. Ruggles-Wrenn, M., Hetrick, G. and Baek, S. [2008], 'Effects of frequency and environment on fatigue behavior of an oxide-oxide ceramic composite at 1200°c', *International Journal of Fatigue* **30**, 502–516.

20. Ruggles-Wrenn, M. and Hilburn, S. [2015], 'Creep in interlaminar shear of an oxide/oxide ceramic-matrix composite at elevated temperature', *Journal of Engineering for Gas Turbines and Power* **138**, 021401–1–021401–8.

21. Ruggles-Wrenn, M. and Lanser, R. [2016], 'Tension-compression fatigue of an oxide/oxide ceramic composite at elevated temperature', *Materials Science Engineering A* **659**, 270–277.

22. Ruggles-Wrenn, M. and Lee, M. [2016], 'Fatigue behavior of an advanced sic/sic ceramic composite with a self-healing matrix at 1300°c in air and in steam', *Materials Science and Engineering A* **677**, 438–445.

23. Ruggles-Wrenn, M., Mall, S., Eber, C. and Harlan, L. [2006], 'Effects of steam environment on high-tempreature mechanical behavior of nextel^{TM} 720/alumina (n720/a) continuous fiber ceramic composite', *Composites Part A: Applied Science and Manufacturing* **37**, 2029–2040.

24. Ruggles-Wrenn MB, Mall S, E. C. H. L. [2006], 'Effects of steam environment on high-temperature mechanical behavior of nextel^{TM} 720/alumina (n720/a) continuous fiber ceramic composite', *Composites Part A: Applied Science and Manufacturing* **37**, 2029–2040.

25. Singh, M. and Asthana, R. [2007], 'Brazing of advanced ceramic composites: Issues and challenges', *Characterization and Control of Interfaces for High Quality Advanced Materials II* .

26. Wilson, M. [2018], Oxidation of SiC/BN/SiC Ceramic Matrix Composites and their Constitutents, PhD thesis, University of Virginia, School of Engineering and Applied Science.

27. Witzgall, S. A. [2020], Tension-tension fatigue behavior of nextel^{TM} 720/alumina-mullite ceramic composite at 1200°c in air and in steam, Master's thesis, Air Force Institute of Technology, Air University, 2950 Hobson Way, Wright-Patterson AFB, OH 45433, United States. An optional note.

28. Zawada, L., Staehler, J. and Steel, S. [2004], 'Consequence of intermittent exposure to moisture and salt fog on the high-temperature fatigue durability of several ceramic matrix composites', *Journal of the American Ceramic Society 86* **86**, 1282–1291.

29. Zok, F. W. and Levi, C. G. [2001], 'Mechanical properties of porous-matrix ceramic composites', *Advanced Engineering Materials* **3**, 14–23.

REPORT DOCUMENTATION PAGE

Form Approved
OMB No. 0704–0188

1. REPORT DATE *(DD–MM–YYYY)*	2. REPORT TYPE	3. DATES COVERED *(From — To)*
25–03–2021	Master's Thesis	August 2019 — March 2021

4. TITLE AND SUBTITLE

Fatigue of two oxide/oxide ceramic matrix composites at 1200°C in air and in steam. Effect of diamond drilled effusion holes.

5a. CONTRACT NUMBER

5b. GRANT NUMBER

5c. PROGRAM ELEMENT NUMBER

6. AUTHOR(S)

Cabri, Anthony R., 2d Lt, USAF

5d. PROJECT NUMBER

5e. TASK NUMBER

5f. WORK UNIT NUMBER

7. PERFORMING ORGANIZATION NAME(S) AND ADDRESS(ES)

Air Force Institute of Technology
Graduate School of Engineering and Management (AFIT/EN)
2950 Hobson Way
WPAFB OH 45433-7765

8. PERFORMING ORGANIZATION REPORT NUMBER

AFIT-ENY-MS-21-M-291

9. SPONSORING / MONITORING AGENCY NAME(S) AND ADDRESS(ES)

Agency of Command Name
POC Rank & Name within Agency
Street Address
City, ST ZIP
email of agency POC

10. SPONSOR/MONITOR'S ACRONYM(S)

11. SPONSOR/MONITOR'S REPORT NUMBER(S)

12. DISTRIBUTION / AVAILABILITY STATEMENT

Approval for public release; distribution is unlimited.

13. SUPPLEMENTARY NOTES

14. ABSTRACT

The tension-tension fatigue behavior of two oxide-oxide ceramic matrix composites (CMCs) was investigated at 1200°C in laboratory air and steam. Both composites consist of a porous oxide matrix reinforced with laminated, woven mullite/alumina (Nextel^{TM}720) fibers. The first composite had an alumina matrix, while the second had an alumina-mullite matrix. First, we assessed the effects of incorporating mullite into the matrix material on fatigue performance by studying the tension-tension fatigue behavior of alumina-mullite matrix CMC. Second, we evaluated the effects of effusion holes on the alumina matrix CMC's fatigue performance. Specimens containing an array of 17 effusion holes of 0.5-mm diameter were tested in tension-tension fatigue. The fatigue run-out was set to 100,000 cycles. All specimens that achieved fatigue run-out were subjected to tension tests to failure in order to measure the retained tensile properties. Fracture surfaces of the tested specimens were examined, damage and failure mechanisms are discussed.

15. SUBJECT TERMS

ceramic matrix composites, tension-tension fatigue, effusion holes and braze joining

16. SECURITY CLASSIFICATION OF:			17. LIMITATION OF ABSTRACT	18. NUMBER OF PAGES	19a. NAME OF RESPONSIBLE PERSON
a. REPORT	b. ABSTRACT	c. THIS PAGE			Dr. Marina B. Ruggles-Wrenn, AFIT/ENY
U	U	U	UU	86	19b. TELEPHONE NUMBER *(include area code)* (937) 255-3636, x4641; marina.ruggles-wrenn@afit.edu